MARTIN MARETTA ENERGY SYSTEMS LIBRARIES
3 4456 0286752 9

CENTRAL RESEARCH LIBRARY
DOCUMENT COLLECTION

ORNL-2731
Physics and Mathematics

STOPPING POWER OF THIN ALUMINUM FOILS FOR 12 TO 127 KEV ELECTRONS

Ford Kalil
W. G. Stone
H. H. Hubbell, Jr.
R. D. Birkhoff

CENTRAL RESEARCH LIBRARY
DOCUMENT COLLECTION
LIBRARY LOAN COPY
DO NOT TRANSFER TO ANOTHER PERSON
If you wish someone else to see this document, send in name with document and the library will arrange a loan.

OAK RIDGE NATIONAL LABORATORY
operated by
UNION CARBIDE CORPORATION
for the
U.S. ATOMIC ENERGY COMMISSION

LEGAL NOTICE

This report was prepared as an account of Government sponsored work. Neither the United States, nor the Commission, nor any person acting on behalf of the Commission:

A. Makes any warranty or representation, expressed or implied, with respect to the accuracy, completeness, or usefulness of the information contained in this report, or that the use of any information, apparatus, method, or process disclosed in this report may not infringe privately owned rights; or

B. Assumes any liabilities with respect to the use of, or for damages resulting from the use of any information, apparatus, method, or process disclosed in this report.

As used in the above, "person acting on behalf of the Commission" includes any employee or contractor of the Commission, or employee of such contractor, to the extent that such employee or contractor of the Commission, or employee of such contractor prepares, disseminates, or provides access to, any information pursuant to his employment or contract with the Commission, or his employment with such contractor.

ORNL-2731

Contract No. W-7405-eng-26

HEALTH PHYSICS DIVISION

STOPPING POWER OF THIN ALUMINUM FOILS FOR 12 TO 127 KEV ELECTRONS

Ford Kalil
W. G. Stone
H. H. Hubbell, Jr.
R. D. Birkhoff

Submitted as a thesis to the Faculty of the Graduate School of Vanderbilt University in partial fulfillment of the requirements for the degree of Doctor of Philosophy in Physics.

DATE ISSUED

SEP 3 1959

OAK RIDGE NATIONAL LABORATORY
Oak Ridge, Tennessee
operated by
UNION CARBIDE CORPORATION
for the
U. S. ATOMIC ENERGY COMMISSION

MARTIN MARIETTA ENERGY SYSTEMS LIBRARIES

3 4456 0286752 9

ACKNOWLEDGMENTS

The authors would like to thank W. Happer for considerable help in taking and calculating the data; R. H. Ritchie for many suggestions and discussions; J. A. Harter, A. Carter, and H. Holzer for their suggestions regarding electric circuitry, and their help in maintenance of the accelerator and their design and construction of the temperature control circuit; J. V. Cathcart and J. J. Campbell of the Metallurgy Division for their help in the preparation of thin foils; P. N. Hensley, R. Jones, and the Health Physics Machine Shop staff for their cooperation and help in making component parts of the apparatus.

One of us (FK) wishes to acknowledge receipt of a United States Public Health Service Research Fellowship which supported him during the course of this research.

TABLE OF CONTENTS

		Page
Acknowledgments		ii
List of Tables		vi
List of Figures		vii
I.	Introduction	1
II.	Previous Measurements of Stopping Power	6
III.	Theory of Stopping Power and Scattering	11
	A. Electron Stopping Power	11
	1. Classical Formulation of Bohr	11
	2. Quantum Mechanical Formulation of Bethe	17
	B. Calculation of Path Length in a Thin Foil	21
	C. The Mean Squared Scattering Angle	25
	1. Williams' Scattering Distribution	25
	2. Molière's Scattering Distribution	29
IV.	Transient Response of the Calorimeter	30
V.	Apparatus and Techniques	38
	A. Accelerator and Auxiliary Equipment	38
	1. The Accelerator Tube	38
	2. High Voltage Power Supply	38
	3. Electron Gun Power Supply	39
	4. Electron Gun	41
	5. Vacuum System	42

TABLE OF CONTENTS (Con't)

				Page
V.	B.	The Determination of $\overline{\Delta E}$		43
		1.	Measurement of i_B	43
			a. Defining Slits and Aiming Screen	46
			b. Bias Discs and Power Supply	46
			c. Current Measuring Circuitry	48
		2.	Measurement of P_B	50
			a. Foil Mounting Ring	50
			b. Thermocouples and Heat Sink	52
			c. Isothermal Furnace and Temperature Control	62
	C.	The Determination of $\overline{\Delta X}$		65
		1.	The Cahn Electrobalance	65
		2.	Modifications to the Electrobalance	69
	D.	Preparation of Foils		71
VI.	Procedure			80
	A.	Measurement of $\overline{\Delta E}$		80
		1.	Determination of K_1 and K_2	80
		2.	Measurement of P_B	88
		3.	Determination of $\overline{\Delta E}$	90
	B.	Measurement of $\overline{\Delta X}$		90
VII.	Results			94
VIII.	Discussion			96
IX.	Conclusions			98

TABLE OF CONTENTS (Con't)

	Page
Appendix	
A. Sample Calculations	100
1. Calibration	100
2. Determination of $\overline{\Delta E}$	105
3. Determination of $\overline{\ell}$	106
B. Summary of Data and Results	111
C. Error Analysis	115
D. List of Symbols Used	118
Bibliography	122

LIST OF TABLES

		Page
I.	Effects of Various Modifications to the Electrobalance	72
II.	Temperature Versus Time for One Calibration Point	101
III.	Calibration Data for Heat Capacity Constant $(K_1)^{-1}$ (50.3 $\mu g/cm^2$ Al Foil)	103
IV.	Calibration Data for Electrobalance	106
V.	Stopping Power Data for the 50.3 $\mu g/cm^2$ Al Foil	112
VI.	Stopping Power Data for the 107.8 $\mu g/cm^2$ Al Foil First Run	113
VII.	Stopping Power Data for the 107.8 $\mu g/cm^2$ Al Foil Second Run	114

LIST OF FIGURES

		Page
1.	Collision Between a Moving Electron and an Electron at Rest	12
2.	Diagram for the Scattering Angles	22
3.	Temperature Versus Time for Constant Beam Current	34
4.	Electron Gun Power Supply	40
5.	Schematic of the Apparatus for Measuring $\overline{\Delta E}$	44
6.	Apparatus for Making Welded Thermocouple Junctions	54
7.	Assembly Drawing of the Thermocouples, Heat Sink and Foil Mount	55
8.	Thermocouple Circuits	59
9.	Control Circuit for Constant Temperature Furnace	61
10.	Schematic of Cahn Electrobalance Model M-10	66
11.	Electrobalance Pan, Arm, and Torque Motor	67
12.	Typical Temperature Versus Time Curves	83
13.	Logarithmic Graph of Temperature Versus Time	85
14.	Calibration Curve: Rate of Temperature Change Versus Absorbed Power	87
15.	Absorbed Power Versus Beam Current for Various Beam Energies	89
16.	Stopping Power of Aluminum (50.3 $\mu g/cm^2$ Foil) and (107.8 $\mu g/cm^2$ Foil)	95

I. INTRODUCTION

Recently the role of stopping power in the induction of chemical and biological effects by radiation has renewed interest on a microscopic scale in the slowing down of charged particles in matter. In addition, dosimetry measurements depend to a large extent on the precision of stopping-power data. The Bragg-Gray principle which is used in dosimetry states that the ratio of energy absorbed in a small volume of dense medium to the energy absorbed in an equal volume of gas is equal to the ratio of their respective stopping powers.

In beta-ray dosimetry, maximum permissible beta-ray exposures are based on the stopping powers of skin. Also, the present calculations of the maximum permissible concentrations of beta-ray emitters in the body are based on a knowledge of the stopping powers of human tissue.

The stopping power of an absorber for electrons is defined as the average spatial rate at which electrons lose energy along a track in passing through an absorbing medium, i.e., the stopping power is $\langle \frac{dE}{dx} \rangle$. In passing through matter a low-energy electron loses energy primarily by collisions with the electrons of the absorbing material. These collisions bring about both excitation and ionization of atoms in the material. In the latter cases, secondary electrons are produced which are indistinguishable from the primary. The electron emerging from a collision with the higher energy is generally called the primary and

thus the maximum energy loss in any one collision in a thin foil is one-half the incident energy. Careful attention to the fate of secondary electrons liberated in a foil must be paid in order that a meaningful measurement of stopping power may be made which will be in accord with the definition of this quantity.

The electron also experiences a number of collisions with the nuclei of the absorber, in which case it is scattered without any appreciable energy transfer because of the relatively large mass of the nucleus compared with that of the electron. Thus in making stopping power measurements, very thin absorbers must be used to minimize multiple scattering so that the electron path length will not be too different from the absorber thickness. If the path length of the electron and the absorber thickness are not too different, then the path length may be calculated with reasonable accuracy from existing multiple-scattering theories.

Effects other than ionization, excitation, and scattering may be neglected for the low-energy electrons being considered here. That is, the reduction of energy loss at high energies due to the shielding effect of the polarization of the medium by the incident electron, and the energy loss by radiation are very much smaller in magnitude than the energy loss by excitation and ionization for energies of the order of a hundred kilovolts or less.

Most experiments on electron stopping power to date have attempted to measure the energy distribution of an electron beam from an approximately monoenergetic source both before and after passage through a thin foil. All such experiments have faced the following dilemma. If the foil is thick enough to give an appreciable difference between the distributions before and after passage through the foil, then multiple scattering renders the path length unknown, and the electrons emerge from the foil with such a wide angular distribution that only a small fraction of the beam may enter the acceptance angle of the electron spectrometer. This fraction is in general not a fair indication of what has happened to the average electron, and the intensity is so low that the count rates in the spectrometer become subject to serious statistical error. If the foil is made thinner in order to avoid the complications introduced by scattering, then the differences between the two distributions become so slight as to introduce appreciable error in the evaluation of the difference in the average energy.

One additional difficulty in the method is due to the shape of the energy loss or straggling distribution which is characterized by a long low-intensity "tail" representing those few electrons which have lost much more than the average amount of energy. Despite their small abundance they represent an appreciable part of the total energy loss. Unfortunately they are lost in the "background count" in the usual spectrometric measurement.

The problems mentioned above may be avoided if the energy delivered to the foil is determined directly by measuring the temperature change of the foil when under bombardment. Here the foil need be only thick enough to be self supporting, for the heating of even the thinnest foil is readily measurable by conventional calorimetric methods.

Measurements were made of the stopping powers of 50.3 $\mu g/cm^2$ and 107.8 $\mu g/cm^2$ Al foils for monoenergetic electrons having energies of 12 KeV to 127 KeV. The foil thicknesses used were near the limit of minimum foil thicknesses for self-supporting foils. It was this limit on the minimum foil thickness which determined the lowest bombarding energy which could be used. That is, the scattering at this lowest energy and the corresponding increase in path length introduced uncertainty in the average path. Had thinner films with a supporting plastic backing been used, then the energy losses of the plastic support would have been an appreciable part of the total measured stopping power.

A cathode-ray gun and linear accelerator were used as the source of monoenergetic electrons. A well-defined beam of electrons impinged normally on the foil surface and passed through the foil. The power dissipated by the electrons losing energy in going through the foil, P_B, was measured calorimetrically. This power is the product of the average energy loss ($\overline{\Delta E}$) and the electron-beam current (i_B). Because the beam was composed of many electrons per second and the observation times were many seconds a direct measurement of the average energy lost by an electron ($\overline{\Delta E}$) in passing through the foil was obtained. The average

foil thickness ($\overline{\Delta x}$) was measured by weighing the foil and measuring its area, to get the foil thickness in units of $\mu g/cm^2$. The increased path length $\overline{\ell}$ of the electron going through the foil was calculated. When the path-length increases were larger than about 30% of the foil thickness, the stopping power measurements were considered invalid. The stopping power was then calculated by taking the ratio $\overline{\Delta E}/\overline{\ell}$.

II. PREVIOUS MEASUREMENT OF STOPPING POWER

Comparatively little work has been done on the measurement of stopping power for low-energy electrons. Leithäuser[1] was the first to observe that electrons lose energy in penetrating thin layers of matter. Early investigators[2] used either cathode rays or internal conversion electrons from radioactive sources, and studied the electron energy loss in many substances including air, Al, Au, Ag, Sn, Cu, and Pt.

These studies were made over a wide energy range of 1 KeV to 1 MeV. Early investigators were not concerned with stopping power as defined here, but rather were attempting to verify the empirical relationship

$$v_o^4 - v_x^4 = a\,x \qquad (1)$$

suggested by Whiddington[3], where v_o is the velocity of the incident electron, v_x is the velocity of the electron after passing through the absorber of thickness x, and "a" is a constant of proportionality which depends on the material and to some extent on the velocity. Little can be concluded about stopping powers from the work of these early experimentors because of excessive scattering, poor resolving power of the apparatus, and distortion of the intensity distributions by the photographic

---

[1] E. Leithäuser, Ann. Phys. Lpz. 15, 299 (1904).

[2] For a discussion of and reference to these early works, see W. Bothe, Handbuch der Physik, Bd. 22/2, 1 (1933).

[3] R. Whiddington, Proc. Roy. Soc. Lond. A-86, 360 (1912).

films which were frequently used as detectors. Also, the v_x referred to the peak rather than the average of the energy loss distribution. The principal value of these early experiments then was to establish the order of magnitude of the effect.

Later investigators[4], using either cathode rays or conversion electrons from radioactive sources, investigated the electron energy loss in a wide range of substances such as A, Al, Ag, Au, Be, Cu, CH_4, Kr, Ne, Pb, Sn, Ta, mica, and organic materials. The foil thicknesses studied varied from about 1 mg/cm^2 to 53 mg/cm^2. The energy range of the incident electrons used was from about 24 KeV to 2 MeV. Some of the radioactive sources used were Cs^{137}, P^{32}, RaB, RaC, Re^{186}, Re^{188}, Se^{75}, Ta^{182}, and ThB.

The general method used by these investigators, with one exception[5,6], was not to measure the energy loss directly but rather to measure the energy distribution of the electrons after passing through the absorber. The usual method for measuring this energy distribution was to use a beta spectrometer in which a variable magnetic field bent the electrons through a slit system and onto a detector. The magnitude of the magnetic field for the particular radius of curvature, as determined by the slit system, gave the electron energy. Detectors used were either photographic films, Geiger counters, or Faraday cups with electroscopes.

---

[4] A discussion of these experiments may be found in R. D. Birkhoff, Handbuch der Physik 34, 53 (1958).

[5] P. Rothwell, Proc. Phys. Soc. Lond. 64, 911 (1951).

[6] D. West, Proc. Phys. Soc. Lond 66, 306 (1953).

By measuring the displacement of the peak of the energy-loss distributions, these investigators were able to determine the most probable energy loss fairly accurately. Their experimental results were compared with the theories of Landau[7] and Blunck and Leisegang[8], who had studied theoretically the problem of the distribution of energy losses for electrons passing through matter. The experimental values of the most probable energy loss agreed quite well with the theory. However, the experimental distributions were usually broader than predicted by theory. Foil thicknesses used in the experiments were relatively large in order to insure energy losses large enough to measure. For this reason and because of the source-foil geometries used, the average path length of the electrons traversing the foil frequently could not be determined. In addition, because of the long tail of the experimental distributions, the average energy loss could not be obtained with any precision. Hence, very little could be said about stopping power $\langle \frac{dE}{dx} \rangle$ from the experiments.

The energy-loss distribution was measured directly by Rothwell[9] and West[10], using monoenergetic electrons selected from a beta continuum by a beta spectrometer. This beam of electrons then went through a

---

[7] L. Landau, J. Phys. USSR, 8, 201 (1944).

[8] O. Blunck and S. Leisegang, Z. Phys. 128, 500 (1950).

[9] P. Rothwell, op. cit.

[10] D. West, op. cit.

proportional counter filled with the gas which constituted the absorber. The counter was cylindrical with a thin mica window on each end of the cylinder. One window was placed as near as possible to the exit slit of the beta spectrometer. An end-window Geiger counter was placed at the other window where the electrons emerged. The two counters were in coincidence so that the coincident pulse opened a gate to permit the delayed proportional counter pulse to go into a four-channel kicksorter. Thus only the electrons passing directly through the proportional counter were counted, and the background count was practically eliminated.

It was assumed that the total ionization produced in the counter by the primary electron and its secondaries was a measure of the energy lost by the primary particle. Hence, the pulse height, which is proportional to the ionization, would be a measure of the energy loss. Calibration was accomplished with K-capture X-rays having energies of 4.95 KeV, 8.05 KeV, 10.5 KeV, and 20.2 KeV from the radioisotopes Cr^{51}, Zn^{65}, Se^{75}, and Pd^{103}. Electron energies greater than 1 MeV were used because the incident electrons entering the counter lost some energy in the mica windows. Since the stopping power is practically constant between 1 Mev and 2 Mev, the resulting pulse height distribution was independent of counter window absorption. In addition, some of the secondary electrons produced in the mica windows entered the counter and produced ionization in the counter. It was assumed that this latter ionization was equal to the ionization lost in the walls of the counter by secondary electrons formed in the counter.

With this method, the distribution of the energy lost in the absorber was measured directly. However, the average energy loss could still not be found because of the collimation used and because of the failure to measure the few large energy losses. Furthermore, the observations were limited to energies greater than 1 MeV because of the energy loss in the mica window. Thus there seemed to be a need for additional studies wherein 1) the average energy loss would be measured directly; 2) there would be no window correction to be applied to the data; 3) the energy deposition of the high energy secondaries or delta rays would be better controlled. That is, an electric field at the foil could reflect the delta rays back into the absorber so that they would deposit their energy there, in contrast to the experiments of Rothwell and West where an equilibrium condition between the secondaries ejected from the window into the counter and the secondaries ejected from the counter into the counter walls had to be assumed.

III. THEORY OF STOPPING POWER AND SCATTERING

A. Electron Stopping Power

1. Classical Formulation of Bohr

In passing through matter an electron is slowed down by collisions with electrons of the material. The elementary classical treatment has been summarized by Birkhoff[11] and will be followed here. Consider an incident electron with an energy much larger than the binding energies of the orbital electrons in the medium. These electrons may then be considered to be essentially free and at rest. Next assume that only a small fraction of the incident energy is transferred to the free electron, as is true in the overwhelming majority of collisions. Then it may be assumed that the incident electron will not suffer an appreciable change in direction, and the calculation is simplified considerably.

In Figure (1) the incident electron is shown moving in the positive x direction. Consider the free electron to be at rest at a distance $\vec{r}$ from the incident electron such that the distance from the free electron to the path of the incident electron will be $r \sin \theta = b$. The quantity b is usually called the impact parameter. Assume that the free electron does not move any appreciable distance during the collision so that b may

[11] R. D. Birkhoff, op. cit.

UNCLASSIFIED
ORNL-LR-DWG. 37724

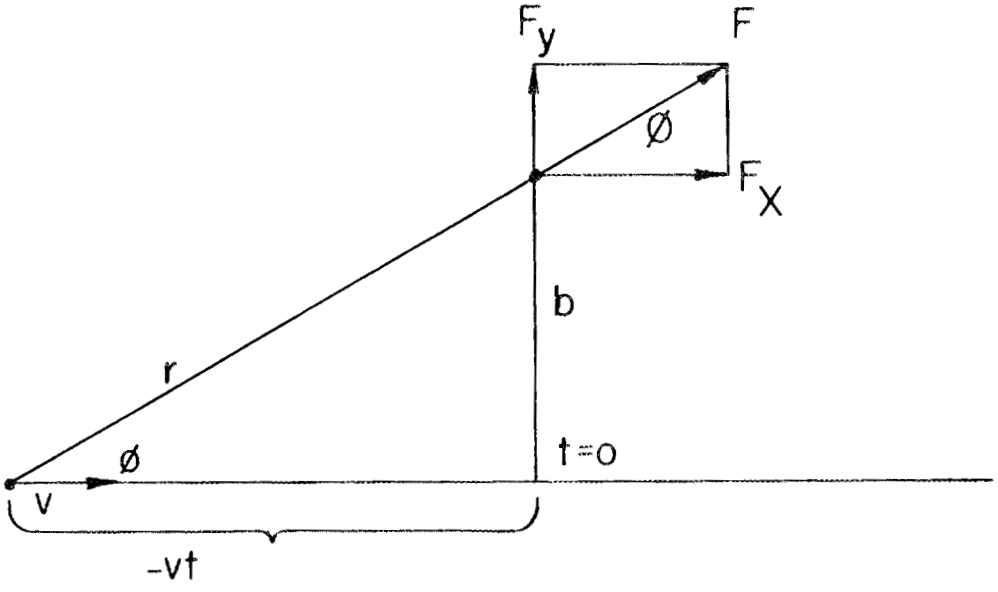

Figure 1. Collision Between a Moving Electron and an Electron at Rest.

be considered to be a constant. The coulomb force between the electrons is repulsive

$$\vec{F} = \frac{e^2}{r^3}\,\vec{r} = m_o\ddot{\vec{r}} \tag{2}$$

and has components

$$F_x = \frac{e^2}{r^2}\cos\theta = m_o\ddot{x} \quad , \tag{3}$$

$$F_y = \frac{e^2}{r^2}\sin\theta = m_o\ddot{y} \quad , \tag{4}$$

where m_o is the electron rest mass. Hence, the components of momentum transferred to the free electron are

$$P_x = \int_{-\infty}^{\infty} F_x\,dt = \int_0^{\pi} \frac{e^2}{r^2}\cos\theta\,\frac{dt}{d\theta}\,d\theta \quad , \tag{5}$$

and

$$P_y = \int_{-\infty}^{\infty} F_y\,dt = \int_0^{\pi} \frac{e^2}{r^2}\sin\theta\,\frac{dt}{d\theta}\,d\theta \quad . \tag{6}$$

Now

$$r = \frac{b}{\sin \theta} \quad , \tag{7}$$

and

$$\cot \theta = \frac{-vt}{b} \quad . \tag{8}$$

Hence,

$$t = -\frac{b}{v} \cot \theta \quad , \tag{9}$$

and

$$\frac{dt}{d\theta} = \frac{b}{v \sin^2 \theta} \quad . \tag{10}$$

Hence,

$$P_x = \frac{e^2}{bv} \int_0^{\pi} \cos \theta \, d\theta = 0 \quad , \tag{11}$$

and

$$P_y = \frac{e^2}{bv} \int_0^{\pi} \sin \theta \, d\theta = \frac{2e^2}{bv} \quad . \tag{12}$$

The energy (W) transferred to the free electron is

$$W = \frac{P_y^{\,2}}{2m_o} = \frac{2e^4}{b^2\, m_o v^2} \quad . \tag{13}$$

The energy W is the energy lost to one electron in a collision. To obtain the energy lost to all electrons of a medium lying in this volume element $d\tau = 2\pi\, b db dx$, W must be multiplied by the number of electrons in $d\tau$. This energy is

$$\frac{2e^4}{m_o v^2\, b^2} \quad 2\pi\, b db dx\, NZ \quad = \quad \frac{4\pi\, NZe^4}{m_o v^2} \quad dx \quad \frac{db}{b}$$

where $N = \frac{N_A \rho}{A}$ = number of atoms per cc, and N_A is Avogadro's number; ρ, Z, and A are the density, atomic number, and atomic weight of the material. To get the stopping power $\frac{dE}{dx}$, the above expression must be integrated over the range of impact parameters between b_{min} and b_{max}; i.e.,

$$-\frac{dE}{dx} = \frac{4\pi\, NZe^4}{m_o v^2} \int_{b_{min}}^{b_{max}} \frac{db}{b} = \frac{4\pi\, NZe^4}{m_o v^2} \ln \frac{b_{max}}{b_{min}} \quad . \tag{14}$$

Hence, to get an expression for stopping power, the maximum and minimum impact parameters must be determined.

In the distant collisions at b_{max}, where the minimum energy transfer will occur, the time of collision is of the order b_{max}/v. If an orbital electron is considered to move like a harmonic oscillator, then its period of motion is of the order of $\frac{1}{\omega}$. Thus the maximum impact parameter is given by

$$\frac{b_{max}}{v} = \frac{1}{\omega} \quad ; \qquad b_{max} = \frac{v}{\omega} \quad . \tag{15}$$

In a more accurate analysis, the electric field of the incident electron appears to the target electron to be an electromagnetic pulse. This pulse may be Fourier analyzed into frequency components. If the transfer of energy occurs at resonance, then the inverse of the lowest Fourier frequency will be of the order of the collision time b_{max}/v. The transfer of energy from the incident to the orbital electrons occurs at resonance, i.e., when the Fourier frequency is equal to the frequency of the orbital electron.

In the classical theory, Bohr took the maximum energy which could be transferred in a single collision to be the energy of the incident electron. In such a case W_{max} becomes $\frac{1}{2} m_o v^2$. Hence

$$W_{max} = \frac{2e^4}{b_{min}^2 \, m_o v^2} = \frac{1}{2} m_o v^2 \quad ,$$

and

$$b_{min} = \frac{2e^2}{m_o v^2} \quad . \tag{16}$$

Then

$$-\frac{dE}{dx} = \frac{4\pi\ NZe^4}{m_o v^2} \ln \frac{m_o v^3}{2e^2\omega} \quad . \tag{17}$$

In a more rigorous calculation, Bohr obtained

$$-\frac{dE}{dx} = \frac{4\pi\ NZe^4}{m_o v^2} \ln \frac{1.123\ m_o v^3}{e^2\omega} \tag{18}$$

2. Quantum Mechanical Formulation of Bethe

The incident electron-atomic electron interaction is an inelastic collision in which the energy transferred to the orbital electron (assumed to be virtually at rest) excites it to higher states. The average energy transferred in a collision is calculated by obtaining the matrix elements for all the transitions of the electron induced by the field of the incident electron and then averaging over all initial and final states. The stopping power of the medium is the sum of the contributions from all its electrons.

In his earlier quantum mechanical treatment, Bethe[12] replaced the single frequency ω by an assemblage of oscillators having frequencies ω_i, and oscillator strengths f_i so that $\sum_i f_i = Z$. Hence, the stopping power formula becomes

$$-\frac{dE}{dx} = \frac{4\pi N e^4}{m_o v^2} \sum_i \int_{b_{min}}^{b^i_{max}} f_i \frac{db}{b} \quad , \tag{19}$$

where

$$b^i_{max} = \frac{v}{\omega_i} \quad . \tag{20}$$

According to quantum theory the minimum impact parameter cannot be less than the de Broglie wavelength. Therefore,

$$b_{min} = \frac{\hbar}{m_o v} \quad . \tag{21}$$

This value of b_{min} is larger than the classical b_{min} for most electron energies. Thus the b_{min} given by Equation (21) is more suitable than

---

[12] H. A. Bethe, Ann. Physik 5, 325 (1930).

the classical b_{min}. Because of the lack of experimental or theoretical information regarding either f_i or ω_i, a mean excitation potential I of a substance is defined as

$$I^Z = \prod_i (\hbar\omega_i)^{f_i} \quad . \tag{22}$$

Then Equation (19) becomes

$$-\frac{dE}{dx} = \frac{4\pi N e^4 Z}{m_o v^2} \ln \frac{m_o v^2}{I} \quad . \tag{23}$$

Equation (23) is essentially correct for non-relativistic incident energies. A correct quantum mechanical treatment given by Bethe[13] used the Mott electron-electron scattering formula, and assumed that the more energetic electron after scattering is the primary electron. The result of this calculation is that

$$-\frac{dE}{dx} = \frac{4\pi N e^4 Z}{m_o v^2} \ln \left(\frac{m_o v^2}{2I} \sqrt{\epsilon/2} \right) \quad , \tag{24}$$

where ϵ is the base of the natural logarithms.

For the relativistic case Bethe[13] used the Möller formula for the electron-electron scattering cross section and obtained

$$-\frac{dE}{dx} = \frac{2\pi N e^4 Z}{m_o v^2}\left\{ \ln \frac{m_o v^2 E}{2I^2 \gamma^2} - (2\gamma-\gamma^2) \ln 2 + \gamma^2 + \frac{1}{8}(1-\gamma)^2 \right\} \qquad (25)$$

where E is the kinetic energy of the incident electron, γ is the Lorentz factor $\sqrt{1-\beta^2}$, $\beta = v/c$ with c the velocity of light.

Using the Thomas-Fermi model of the atom, Bloch[14] has developed a theory showing that the mean excitation potential is proportional to Z, i.e.,

$$I = K Z \qquad (26)$$

where K is a constant. Using the more accurate Thomas-Fermi-Dirac model of the atom, which takes into account the electron-spin interactions, Jensen[15] found that

$$I_o = K_o (1 + k_o Z^{-2/3}) Z \quad , \qquad (27)$$

where the index o refers to isolated atoms. The constants K_o and k_o have not been calculated except that $k_o < 0.8$. As Brandt[16] points out,

---

[13] H. A. Bethe, Handbuch der Physik 24, S-273 (1933).

[14] F. Bloch, Z. Phys. 81, 363 (1933).

[15] H. Jensen, Z. Phys. 106, 620 (1937).

[16] W. Brandt, Health Physics 1, 11 (1958).

the constants K_o and k_o must be determined experimentally. Brandt[17] has given a rather detailed discussion of the mean ionization potential. By using the I = 150 ev for aluminum and a Lindhard-Scharff diagram, Brandt gets K_o = 7.6 ev and k_o = 0.6. Such values are difficult to verify for the following reasons. The value of I occurs under the logarithm in the stopping power formula which makes its evaluation by measuring stopping power very difficult. Furthermore, if the stopping power of heavy particles is determined experimentally, the effects of the tightly bound, fast-moving inner shell electrons which do not participate fully in slowing down relatively slow-moving heavy particles must be removed from the data before the Bethe formula is applied. And if the stopping power of electrons is measured, scattering and straggling introduce enough error to make a determination of I all but impossible.

B. Calculation of Path Length in a Thin Foil

In passing through matter electrons are scattered by the nuclei of the stopping material. In most collisions the scatter angle θ per collision is small enough that $\sin\theta \cong \theta$. Also electron-electron scattering is small. Shown in Figure (2) is the scattering geometry in three dimensions. Consider first the triangle ABC, and let OA be dS

[17] W. Brandt, Phys. Rev. 104, 691 (1956).

UNCLASSIFIED
ORNL-LR-DWG. 37725

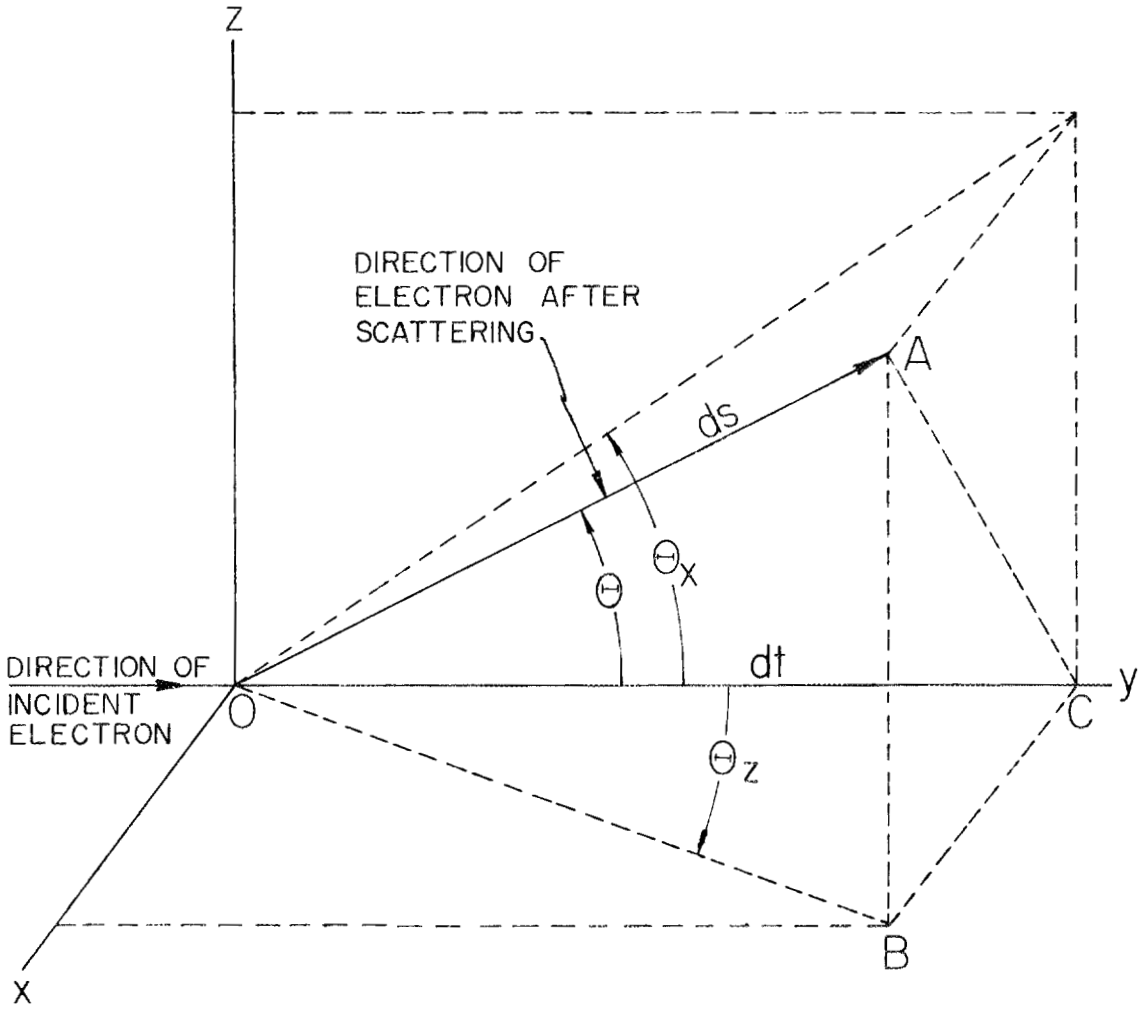

Figure 2. Diagram for the Scattering Angles.

the incremental path length taken by the scattered electron. Then

$$\begin{aligned} AB &= \theta_x \, dS \quad , \\ BC &= \theta_z \, dS \quad , \\ \text{and } AC &= \theta \, dS \quad . \end{aligned} \tag{28}$$

By the Pythagorean theorem,

$$(AC)^2 = (AB)^2 + (BC)^2 \quad . \tag{29}$$

Hence,

$$\theta^2 = \theta_y^2 + \theta_z^2 \tag{30}$$

and

$$\overline{\theta^2} = \overline{\theta_y^2 + \theta_z^2} \tag{31}$$

It can be readily seen that

$$ds = \frac{dt}{\cos \theta} = \frac{dt}{1 - \frac{\theta^2}{2} + \ldots} = dt \left(1 + \frac{\theta^2}{2} - \ldots\right) \tag{32}$$

Since it was assumed that θ is small, terms containing θ to larger powers than 2 may be omitted. Now

$$ds = dt + d\ell \tag{33}$$

where $d\ell$ is the increase in path length due to scattering. Equations (32) and (33) may be solved for $d\ell$

$$d\ell = \frac{\theta^2}{2} dt \quad , \tag{34}$$

so that

$$\overline{d\ell} = \frac{\overline{\theta^2}}{2} dt \quad . \tag{35}$$

Then the total increase in path length $\Delta\ell$ is given by

$$\Delta\ell = \int_0^t d\ell = \frac{1}{2} \int_0^t \overline{\theta^2} \, dt \quad , \tag{36}$$

where t is the foil thickness. The problem then is to calculate the $\overline{\theta^2}$ in Equation (36). To do this, the theory of multiple nuclear scattering must be used as presented in the following section.

C. The Mean Squared Scattering Angle

1. Williams' Scattering Distribution

A simplified treatment of multiple scattering has been given by Williams[18] and will be followed here.

The Rutherford differential cross section per atom for single scattering into a solid angle $d\Omega$ is given by

$$d\sigma(\theta) = \frac{\pi Z^2 e^4 (1-\beta^2)}{2 m_o^2 v^4} \frac{\sin\theta}{\sin^4 \frac{\theta}{2}} d\theta \tag{37}$$

where the rest mass of the electron has been replaced by the relativistic mass. The scattering cross section for small angles may be written as the probability for a single scattering between θ and $\theta + d\theta$ in a thickness dx,

$$f(\theta, dx)d\theta = \frac{8\pi N Z (Z+1) e^4 (1-\beta^2)}{m_o^2 v^4} \frac{d\theta}{\theta^3} dx \quad , \tag{38}$$

where the factor Z^2 is replaced by $Z(Z + 1)$ to account for the scattering by the atomic electrons. Since θ^3 appears in the denominator, the probability for scattering at small angles becomes extremely large. Physically it is the screening of the nuclear charge by the orbital electrons which

[18] E. J. Williams, Proc. Roy. Soc. Lond. A-169, 531 (1939); Phys. Rev. 58, 292 (1940).

reduces the small angle scattering. However, it is sufficient for purposes of integration to cut off the multiple scattering contributions at some minimum angle θ_{min}. Thus, the form of Equation (38) need not be altered. If the Born approximation is valid, i.e., if the amplitude of the scattered wave is small compared to the amplitude of the undisturbed incident wave, then a reasonable estimate of θ_{min} is given by

$$\theta_{min} = \frac{\lambda\!\!\!^{-}}{a} , \tag{39}$$

where

$$\lambda\!\!\!^{-} = \frac{\hbar}{p} \tag{40}$$

and

$$a = a_o Z^{-1/3} \tag{41}$$

In these expressions, p is the momentum of the incident electron, and "a" is the effective shielding radius which is used in the approximate expression for the shielded nuclear potential

$$V = \frac{Z e^2}{r} e^{-r/a} \tag{42}$$

and a_o is the Bohr radius $= \frac{\hbar^2}{m_o e^2} = 5.29 \times 10^{-9}$ cm. (43)

For the above expression for θ_{min} to be valid, the Born approximation requires that

$$\alpha = \frac{Ze^2}{hv} = \frac{Z}{137\,\beta} \ll 1. \tag{44}$$

When this condition is not satisfied, then the classical

$$\theta_{min} = \alpha \frac{\lambda\!\!\!^{-}}{a} \tag{45}$$

is more nearly correct. This expression may be obtained from the equation derived in classical single nuclear scattering theory relating the scattering angle θ and the impact parameter b is the shielding radius a is used for b.

$$\tan \frac{\theta}{2} = \frac{Ze^2}{m_o v^2\, b} \tag{46}$$

The maximum angle of scattering in a single collision (θ_{max}) must now be estimated before $\overline{\theta^2}$ can be evaluated from $f(\theta, dx)$. An arbitrary value of θ_{max} is usually chosen such that there is on the average throughout the whole foil thickness t only one collision in which θ is greater

than θ_{max}. By integrating $f(\theta)$ from θ_{max} to some larger angle θ', where $(\theta')^2 \gg \theta^2_{max}$, and setting the integral equal to unity, the following expression for θ_{max} is obtained,

$$\theta_{max} = \left[t \frac{4\pi N Z (Z+1) e^4 (1-\beta^2)}{m_o^2 v^4} \right]^{1/2} . \tag{47}$$

Equation (38) may then be written as

$$f(\theta,dx)\, d\theta = 2 \frac{\theta^2_{max}}{t} \frac{d\theta}{\theta^3} dx , \tag{48}$$

where $f(\theta,dx)d\theta$ is the single scattering distribution for a thickness dx. Hence

$$\overline{\theta^2}(dx) = \int_{\theta_{min}}^{\theta_{max}} \theta^2 f(\theta,dx)d\theta = 2\theta^2_{max} \ln \frac{\theta_{max}}{\theta_{min}} \frac{dx}{t} , \tag{49}$$

and because of the additivity of mean squared deviations for independent events the total mean squared deviation for a foil of thickness t is $\overline{\theta^2} = 2\theta^2_{max} \ln \frac{\theta_{max}}{\theta_{min}}$. Thus

$$\theta^2 = t \frac{4\pi NZ(Z+1)e^4(1-\beta^2)}{m_o^2 v^4} \ln \left[4\pi Z^{1/3} (Z+1) Nt \left(\frac{h}{m_o v} \right)^2 \right] . \tag{50}$$

2. Moliere's Scattering Distribution

The theory of multiple scattering has been treated most recently by Molière[19] who has considered modifications to the scattering distribution from singly and plurally scattered electrons as well. The value of the mean squared scattering angle differs little from the Williams' value as will be noted below. Solving for $\overline{\theta^2}$, Molière found that

$$\overline{\theta^2} = 2\theta^2_{max} \left[\ln \frac{\theta_{max}}{\theta_{min}} - .289 \right] \tag{51}$$

(compare with Equation 49).

For θ_{max} and θ_{min} Molière used

$$\theta^2_{max} = t \frac{4\pi N Z^2 e^4 (1-\beta^2)}{m_o^2 v^4} , \tag{52}$$

and

$$\theta^2_{min} = \left(\frac{\lambda}{0.885a} \right) (1.13 + 3.76 \alpha^2) . \tag{53}$$

The expression for θ_{max} is similar to that of Williams except that $Z(Z+1)$ is replaced by Z^2. Also, the expression for the angle θ_{min} is similar to that of Williams' except for a slight correction in the Thomas-Fermi radius and for a factor which accounts for deviations from the Born approximation for values of $\alpha = Z/137\beta$ not small compared with unity.

---

[19] G. Molière, Z. Naturforsch, 3a, 78 (1948).

IV. TRANSIENT RESPONSE OF THE CALORIMETER

Consider a well-defined electron beam of circular cross section and of constant beam current impinging normally on the surface of a foil which has been pre-cooled to a temperature T_i below the environmental temperature T_o. Assume that there is some means for measuring the foil temperature at its periphery such as a set of thermocouples equally spaced around the circumference of the foil. Then the time rate of temperature change of the foil, $\dot{T}$, will be proportional to the net heat to the foil per unit time. Hence,

$$\dot{T} = K_1 P_B - K_2(T-T_o) \quad , \tag{54}$$

where T is the foil temperature, $P_B = \overline{\Delta E_B}\, i_B$ = beam power absorbed by the foil in watts, $\overline{\Delta E_B}$ is the average beam energy absorbed by the foil in volts, and i_B is the beam current in amperes.

K_1 is the calibration constant of the system and is equal to the reciprocal heat capacity of the system in appropriate units. $K_2(T-T_o)$ represents the heat exchange between the system and the environment due to conduction and radiation. Because of the small temperature differences involved, the radiation losses are proportional to $T-T_o$ in accord with Newton's law of cooling.

From Equation (54) it can be seen that at $T = T_o$, the rate of temperature change is just

$$\left[\dot{T} \right]_{T_o} = K_1 P_B \tag{55}$$

However, in order to measure $\dot{T}$, the temperature change must be observed for an increment of time $2\Delta t$. Assume that $T = T_o$ at the time t_o, and that the temperature is measured for equal intervals of time, say Δt, on either side of t_o. The problem then is whether or not this observed slope is the same as or nearly the same as the true slope at T_o. If the observed slope is nearly equal to the true slope, then the observed slope may be used a s a direct measure of the beam power absorbed in the foil. If the beam current is known then the average energy loss in the foil $\overline{\Delta E_B}$ may be determined.

By separation of variables and integration of Equation (54) the following result is obtained,

$$\int_{T_i}^{T} \frac{dT}{K_1 P_B - K_2(T-T_o)} = \int_{o}^{t} dt \quad . \tag{56}$$

Let $u = K_1 P_B - K_2(T-T_o)$ so that $du = - K_2 \, dT$. Then

$$t = - \frac{1}{K_2} \int_{T_i}^{T} \frac{du}{u} = - \frac{1}{K_2} \ln \frac{K_1 P_B - (T-T_o) K_2}{K_1 P_B - (T_i-T_o) K_2} \quad , \tag{57}$$

and

$$t_o = -\frac{1}{K_2} \ln \frac{K_1 P_B}{K_1 P_B - (T_i - T_o) K_2} \quad . \tag{58}$$

From Equation (57) it is found that

$$\left[K_1 P_B - (T_i - T_o) K_2 \right] e^{-K_2 t} = K_1 P_B - (T - T_o) K_2 \quad , \tag{59}$$

so that

$$K_2 T = K_1 P_B (1 - e^{-K_2 t}) + K_2 T_o (1 - e^{-K_2 t}) + K_2 T_i e^{-K_2 t} \quad . \tag{60}$$

Hence,

$$T = \left(\frac{K_1}{K_2} P_B + T_o \right) \left(1 - e^{-K_2 t} \right) + T_i e^{-K_2 t} \quad . \tag{61}$$

As a check on this solution for T, it is seen that at $t = 0$, $T = T_i$; and as $t \to \infty$, then

$$T = \frac{K_1}{K_2} P_B + T_o \equiv T_\infty \tag{62}$$

If this definition of T_∞ is used, Equation (61) becomes

$$T = T_\infty (1 - e^{-K_2 t}) + T_i e^{-K_2 t} \quad , \tag{63}$$

or

$$T = T_\infty - (T_\infty - T_i)\, e^{-K_2 t} \quad . \tag{64}$$

Now define $T = T_+$ when $t = t_o + \Delta t$, and define $T = T_-$ when $t = t_o - \Delta t$, so that

$$T_+ = T_\infty - (T_\infty - T_i)\, e^{-K_2(t_o + \Delta t)} \quad , \tag{65}$$

and

$$T_- = T_\infty - (T_\infty - T_i)\, e^{-K_2(t_o - \Delta t)} \quad . \tag{66}$$

As can be seen from Figure (3), the observed or apparent slope is given by

$$\left[\dot{T}\right]_{T_o} = \frac{T_+ - T_-}{2\Delta t} = \frac{(T_\infty - T_i)\left(e^{-K_2(t_o - \Delta t)} - e^{-K_2(t + \Delta t)}\right)}{2\Delta t}$$

$$= \frac{e^{-K_2 t_o}}{2\Delta t}\,(T_\infty - T_i)\left(e^{+K_2 \Delta t} - e^{-K_2 \Delta t}\right) \tag{67}$$

$$= e^{-K_2 t_o}\,\frac{(T_\infty - T_i)}{\Delta t}\,\sinh K_2\,\Delta t \quad .$$

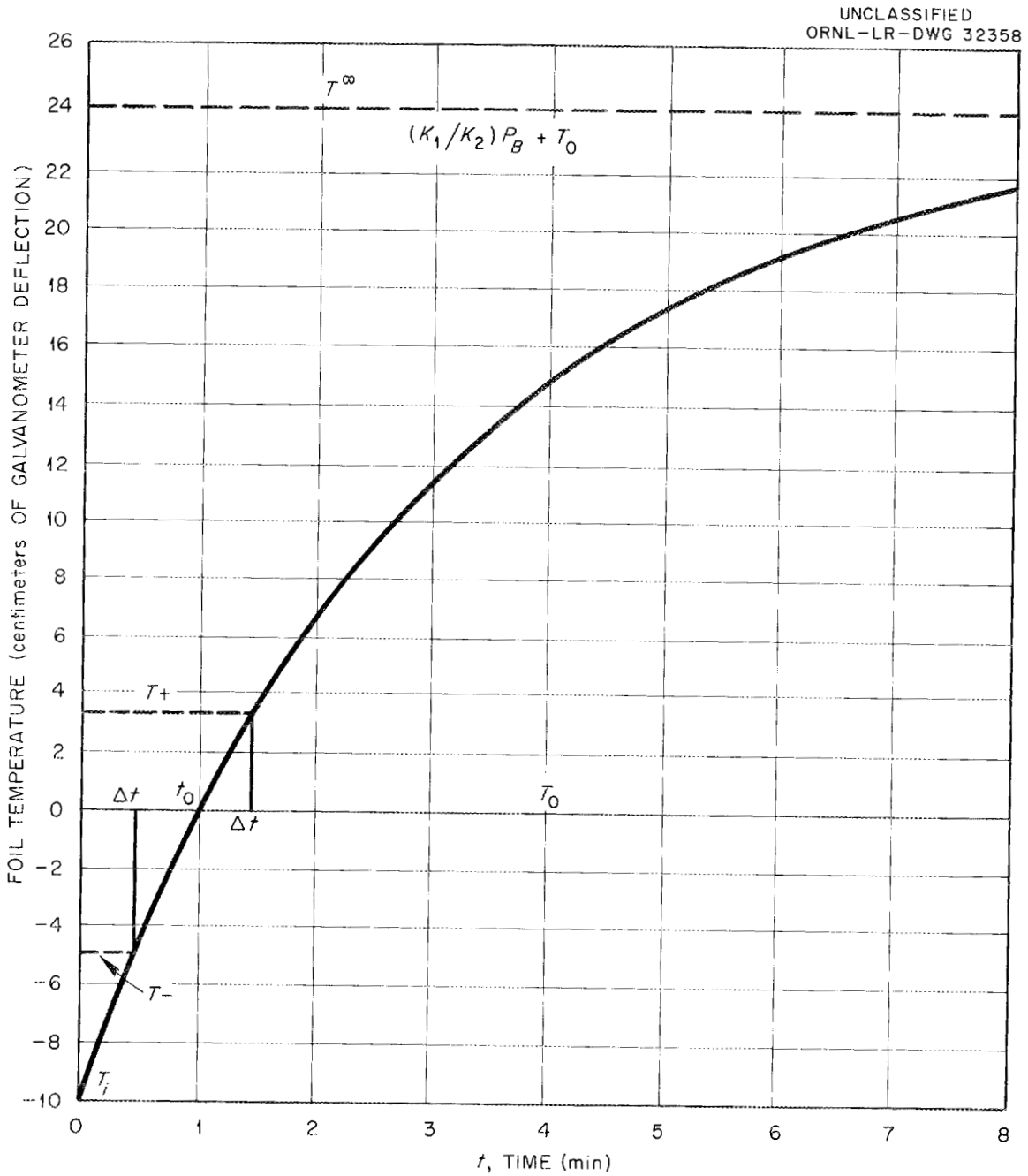

Figure 3. Temperature Versus Time for Constant Beam Current.

From the expression for t_o given in Equation (58), $\dot{T}$ becomes

$$\left[\dot{T} \right]_{T_o} = \frac{K_1 P_B}{K_1 P_B - (T_i - T_o) K_2} \frac{(T_\infty - T_i)}{\Delta t} \sinh K_2 \Delta t \quad . \tag{68}$$

From the expression for T_∞ given in Equation (62) $\left[\dot{T} \right]_{T_o}$ becomes

$$\left[\dot{T} \right]_{T_o} = \frac{K_1 P_B}{K_1 P_B - (T_i - T_o) K_2} \frac{\left(\frac{K_1}{K_2} P_B + T_o - T_i \right)}{\Delta t} \sinh K_2 \Delta t. \tag{69}$$

Factoring out $K_1 P_B - (T_i - T_o) K_2$ in the numerator, Equation (69) becomes

$$\left[\dot{T} \right]_{T_o} = K_1 P_B \frac{\sinh K_2 \Delta t}{K_2 \Delta t} \quad . \tag{70}$$

The $\sinh K_2 \Delta t$ may be expanded to give

$$\sinh K_2 \Delta t = K_2 \Delta t + \frac{(K_2 \Delta t)^3}{3!} + \frac{(K_2 \Delta t)^5}{5!} + \ldots \tag{71}$$

If all but the first term may be neglected, i.e., if

$$K_2 \Delta t \gg \frac{(K_2 \Delta t)^3}{3!} \tag{72}$$

or

$$(K_2 \Delta t)^2 \ll 6 \quad , \tag{73}$$

then

$$\left[\dot{T} \right]_{T_o} \cong \frac{K_1}{K_2} P_B \frac{K_2 \Delta t}{\Delta t} = K_1 P_B = \dot{T}_{true} \quad . \tag{74}$$

The problem now is to determine K_2 which is the reciprocal of the time constant of the sytem. Referring to Equation (61) it can be seen that

$$T = T_o (1 - e^{-K_2 t}) + T_i e^{-K_2 t} \quad , \tag{75}$$

or

$$T = T_o + (T_i - T_o) e^{-K_2 t} \quad , \quad \text{when } P_B = 0 \quad . \tag{76}$$

Then

$$\log_{10} \frac{T - T_o}{T_i - T_o} = - K_2 t \log_{10} \epsilon \quad . \tag{77}$$

Thus, if the pre-cooled foil is permitted to drift toward T_o, K_2 may be evaluated by measuring T as a function of time and by then determining the slope of a plot of $\log_{10} \frac{T - T_o}{T_i - T_o}$ versus t. This slope is equal to $-K_2 \log_{10} \epsilon = - 0.435 K_2$.

The constant K_1 may be determined by decreasing the beam energy until the beam is completely absorbed in the foil. From the measured values of $\left[\dot{T} \right]_{T_o}$, beam energy, and beam current, the constant K_1 may be found.

V. APPARATUS AND TECHNIQUES

A. Accelerator and Auxiliary Equipment

1. Accelerator

An accelerator was used as a monoenergetic source of electrons. The accelerator has been described in a somewhat modified form by Blackstock, Birkhoff, and Slater[20]. It consists of electron gun, an accelerating tube, and another identical tube which may be used for either acceleration or deceleration. In this work, the latter tube was grounded and served no useful purpose. The accelerator tubes are similar to those used in Cockroft-Walton machines and consist of alternate ceramic insulators and accelerating electrodes sealed vacuum tight with vinyl cement.

A voltage divider consisting of six fifty megohm IRC resistors in series and across the accelerating tube was used to establish the electrode potentials.

2. High Voltage Power Supply

The high voltage was supplied by a Westinghouse 250 KV X-ray power supply which was center-grounded to provide flexibility of operation and to permit voltages of 250 KV with no part of the system being more than 125 KV from ground. This power supply was

[20] A. W. Blackstock, R. D. Birkhoff, and M. Slater, Rev. Sci. Inst., 26, 274 (1955).

used for both an X-ray machine and the accelerator. An oil immersed, high voltage switch allowed the power supply to be switched easily to either the X-ray machine or the accelerator. Separate control systems permitted the high voltage supply to be operated from either the accelerator or X-ray control panels. In the work described here the potential applied to the accelerator was varied from 10 to 125 KV. The voltmeter circuit used for measuring the high voltage applied to the accelerator consisted of a calibrated 2% panel meter in series with a string of forty-two calibrated resistors of 4 MΩ each. The resistors were immersed in an oil tank and were calibrated with a Wheatstone bridge to an accuracy of 0.025%. Hence, the relative error of the total resistance of the resistors in series is at least as good as 0.025% and probably as good as $\frac{0.025}{\sqrt{42}}$%. This was much better than the accuracy with which the panel meter can be read, which was about ± 0.5 KV.

Frequently a ± 1%, 30 KV, electrostatic voltmeter was also used to measure the lower potentials applied to the accelerator. Its readings checked very closely with those of the panel meter.

3. Electron Gun Power Supply

Shown in Figure (4) is the power supply for the electron gun. Dual potentiometers (R-8 and R-9) were used to vary the potentials of each member of the two pairs of deflection plates above and below the second anode potential. Panel meters were built into the power supply so that

UNCLASSIFIED
ORNL-LR-DWG. 37741

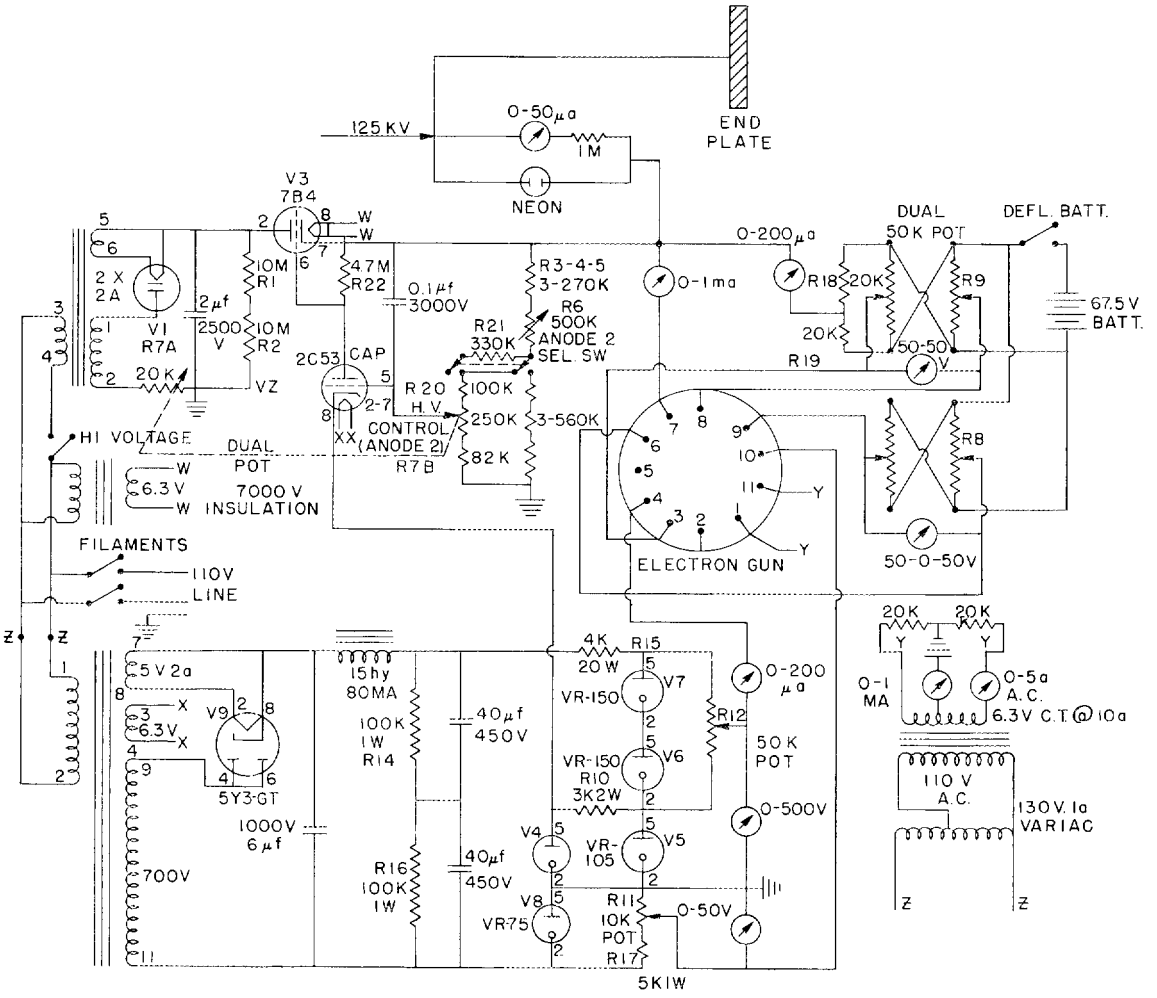

Figure 4. Electron Gun Power Supply.

all of the voltages of and the currents to all of the gun elements could be measured. The electron beam could be aimed by varying the potentials of the deflection plates and the focusing electrodes of the gun in conjunction with the adjustment of the horizontal and vertical magnetic degaussing fields. Most frequently, however, the deflection battery switch was left open and the electron beam was aimed by varying the horizontal and vertical magnetic degaussing fields and the potentials of the focusing electrodes of the electron gun. A Variac was used for controlling the current through the filament of the electron gun.

The chassis of the electron gun power supply was left "floating" and the second anode was connected to the 125 KV power supply and to the end plate of the accelerator. In this manner the gun cathode was at a potential equal to the second anode voltage below the end plate of the accelerator. Hence the electrons from the gun entered the accelerator with a kinetic energy determined by the second anode voltage. Two cascaded isolation transformers were used to supply the 110 AC line voltage to the electron gun power supply.

4. Electron Gun

The electron gun was that used in a General Electric 5BPI cathode ray tube. The guns were purchased on a special order. They were delivered without the luminous screen and cut off at the end of the glass neck. After exposure to air and after each shut-down, the cathode had to be re-activated. This was done in the following manner.

The electron gun and high voltage power supplies were initially off, and the pressure in the accelerator was of the order of 10^{-5} mm of mercury with no liquid nitrogen in the cold traps of the vacuum system. In the electron gun power supply, the filament Variac was set at zero, the second anode switch was turned off, the first and second anode controls were set for minimum potential, and the grid control was set for maximum potential. Then the electron gun power supply was turned on. The filament Variac was adjusted until 0.3 amperes of filament current was obtained. The second anode switch was turned on. Under these conditions there were 450 volts, 150 volts, and -50 volts on the second anode, first anode, and grid respectively. A potential of about 20 KV was then applied to the accelerator. The grid potential of the electron gun was set at zero, and the current through the gun filament was gradually increased to 0.7 amperes. Several minutes of warm-up time were allowed to elapse. The cathode emission meter would then read from 0.6 to 1.0 milliamperes. The beam was then aimed and focused until it was detected at the opposite end of the accelerator. If necessary, the filament current was increased further. However, this was avoided whenever possible in order to prolong the life of the oxide coated cathode.

5. Pumping System

The pumping system used with the accelerator consisted of a small and a large Duo-Seal vacuum pump and an oil diffusion pump. The large Duo-Seal pump and the VMF260 diffusion pump could be

sealed off from the accelerator tubes with a valve. This arrangement made it possible to let air into the accelerator without having to turn off these pumps. The small Duo-Seal pump was used as a roughing pump. With the large Duo-Seal and the diffusion pumps, pressures of 0.3 to 0.5×10^{-5} mm of mercury were obtained. Liquid nitrogen was used in a cold trap between the accelerator and the diffusion pump.

B. The Determination of $\overline{\Delta E}$

As stated earlier, the average energy loss $\overline{\Delta E}$ is given by

$$\overline{\Delta E} = \frac{P_B}{i_B} \tag{78}$$

where P_B is the beam power absorbed by the foil in watts, and i_B is the beam current in amperes. The apparatus for measuring $\overline{\Delta E}$ consisted of two parts, one part for measuring i_B and the other part for measuring P_B.

1. Measurement of i_B

Shown in Figure (5) is a drawing of the apparatus for defining the electron beam and measuring the beam current i_B. It consisted of: a) Defining slits and aiming screen; b) Bias discs and a power supply to provide the bias potential; c) Faraday cup; d) The current measuring apparatus; and e) Electrostatic shield.

UNCLASSIFIED
ORNL-LR-DWG. 37726

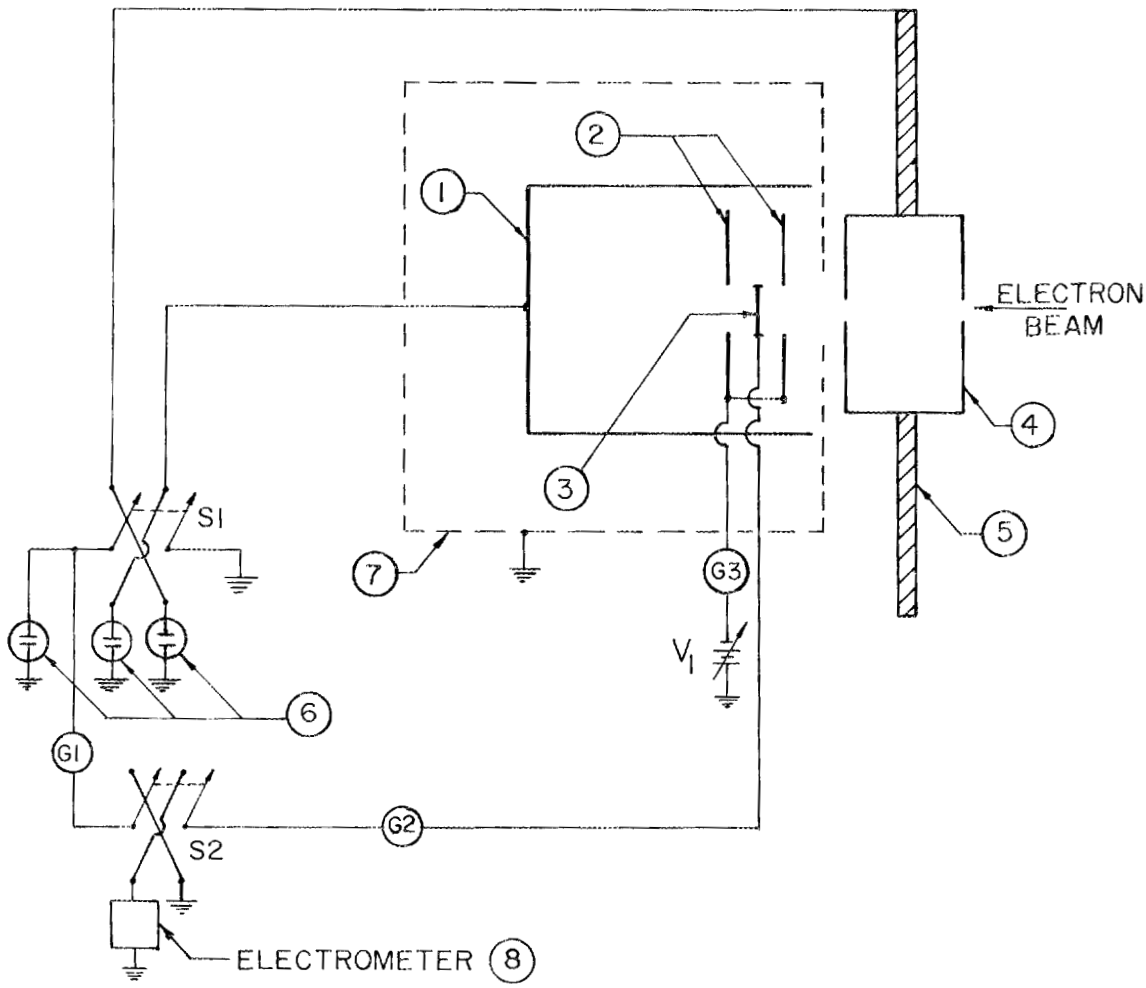

Figure 5. Schematic of the Apparatus for Measuring $\overline{\Delta E}$.

Parts List for Figure 5

Item No.	Description
1.	Faraday cup
2.	Bias Discs
3.	Foil and Foil Mount
4.	Defining Slits, gold-plated aluminum
5.	Aiming Screen
6.	87 Volt, Glow Discharge Tubes
7.	Electrostatic Shield
8.	Keithley Model 410 Micro-microammeter, Keithley Instruments Company, Cleveland, Ohio

V_1 = Negative Power Supply

G1 = Rubicon Galvanometer (X16019), 0.00406 μa/mm sensitivity, 1053 internal resistance

G2 = Leeds and Northrup Galvanometer (X49375), 0.000424 μa/mm sensitivity, 510 internal resistance

a. Defining Slits and Aiming Screen

The holes in the defining slits were 5/16 inch in diameter and the distance between them was adjusted so that the electrons could not hit the foil mounting. Had electrons been able to strike the foil mounting, they would have been completely absorbed, and an erroneous stopping power measurement would have been inferred. In addition, the defining slits were adjusted so that the center of the defined electron beam hit the center of the foil. The aiming screen, made of gold-plated aluminum, was six inches in diameter and 1/2 inch thick. Its function is to facilitate finding and aiming the electron beam. It was made of aluminum, a low Z material, in order to minimize the production of X-rays by the incident electrons. Efforts were made to minimize the production of X-rays in order to reduce emission of electrons from various parts of the apparatus which might cause erroneous current measurements. The surface was gold plated to hide the layer of aluminum oxide. Such a layer could have charged up to produce an extraneous electric field.

b. Bias Discs and Power Supply

The bias discs were made from a brass screen having a fine mesh. Screen was used so that the air would not "blow out" or break the foil when the system was pumped down. Fine mesh was used to minimize distortions of the electric field. Each bias disc was electrically insulated from and mounted on the inside of the Faraday cup. Three small spacers, made of teflon and equally spaced around the circumference

of each bias disc, were used for this purpose. There were two reasons for mounting the bias discs using three small equally spaced insulators rather than a single circular insulator. The first was to permit the air to flow more freely when the system was being pumped down to help prevent breaking the foil. The second was to minimize the insulation surface charge effects which would distort the electric field produced by the bias discs.

The bias discs provided an electric field to repel the secondary electrons which left the foil back into the foil. This was so that secondary electrons would dissipate their energy in the foil in accordance with the definition of stopping power. That is, the primary electron is taken to be the one emerging from the foil with the higher energy. Thus any electron emerging from the foil with less than half the primary energy is assumed to be a secondary and should be reflected back to the foil where it should give up its energy. In addition the bias discs provided an electric field near the Faraday cup to repel the secondary electrons from the Faraday cup back into the cup.

The power supply (V_1) for the bias discs was an Atomic Instrument Company Super-Stable High Voltage power supply with a negative output voltage which could be varied from 0 to -1500 volts in steps of 87 volts. When it was desired to vary the bias disc potential from 0 to -87 volts continuously, a 100 KΩ helipot was used as a continuous voltage divider to give the desired pltential. The output current

of the power supply was kept below 1 ma by use of the 100 K helipot which was the largest available. On occasion another Atomics Instrument Company regulated high voltage power supply was used with a negative output voltage which could be varied from -500 to -3000 volts.

c. Current Measuring Circuitry

A galvanometer (G3) having a sensitivity of 0.000424 microamperes per millimeter was used to measure the current to the bias discs. Galvanometer G2 with a sensitivity of 0.00389 micro amperes per millimeter was used to measure the current to the foil. Depending on the position of the switch SI, galvanometer GI measured the current to either the aiming screen or the Faraday cup. This galvanometer had a sensitivity of 0.00406 micro-amperes per millimeter. These galvanometers had built-in scales, and could be read within $\pm$ 0.2 millimeter. Each galvanometer was frequently calibrated by connecting it in series with a calibrated resistance, and by then measuring the current through the galvanometer by measuring the potential drop across this resistance with a potentiometer.

A reversing switch (52) was used to connect a recording electrometer in series with either galvanometer G1 or galvanometer G2. This was done for two reasons. One was to provide more sensitive current measurements whenever necessary. The other was to provide a permanent record of the beam current, which consisted of the cup current when the stopping measurements were made and the foil current when the beam was completely

absorbed in the foil during the calibration measurements. The electrometer was a Keithley Instruments, Inc., model 410 "Micro-Microammeter", and had 20 overlapping ranges of 10^{-3} to 3×10^{-13} amperes full scale.

The accuracy of the electrometer on the ranges from 10^{-3} through 3×10^{-7} amperes was within 2% of full scale. On the ranges from 10^{-8} through 3×10^{-13} its accuracy was within 4%. It was calibrated at the beginning and end of a day's run by connecting a 1.5 volt dry cell in series with a calibrated wire wound resistance and the electrometer input. The ratio of the voltage drop across the resistance to the resistance gave the current to the electrometer input. This current was compared with the electrometer current measurement as recorded by the Brown recorder, which was always connected to the electrometer output to record the electrometer measurements.

The Brown recorder was a potentiometer-rebalance type recorder which automatically recalibrated itself every few minutes. It was manufactured by the Brown Instrument Company and had a quoted accuracy of 0.25% of full scale deflection.

The potential drop across the calibrated wire-wound resistor was measured with a Leeds and Northrup, type K2 potentiometer. The accuracy of this potentiometer was within one microvolt. Thus, the accuracy of the calibration, and hence the accuracy of the electrometer measurements were within 0.5%, since the electrometer was calibrated on the range used.

The input impedance of the electrometer was controlled by negative feedback from the output so that the total voltage drop across the input terminals was less than 5 millivolts for full scale deflection. On the 10^{-6} ampere scale, which was the largest scale used, the effective input impedance was 5000 ohms. This effective input impedance was thus comparable to galvanometer impedances. The zero drift on all but the most sensitive range was less than 2% in eight hours for a warmup from a cold start. When a two-hour warmup was provided, the zero drift was considerably less. For this reason, the electrometer was left on at all times. Electrometer grid current was less than 5×10^{-14} amperes.

Although the electrometer had a voltage-regulating Sola transformer built into its chassis, an additional sine wave Sola regulator was used for its power supply to minimize harmonics in the power input.

2. Measurement of P_B

The apparatus for measuring the amount of power (P_B) dissipated by the electron beam in the foil consisted of: a) A foil and mounting ring; b) thermocouples and isothermal furnace and heat sink; and c) temperature control.

a. Foil Mounting Ring

The foils were mounted on a small copper ring which had an inside diameter of 0.5 inch and a maximum outside diameter of 0.588 inch at one end, which tapered down to 0.560 inch over a thickness of 3/32 inch.

Three holes equally spaced around the periphery were drilled and tapped for 0-80 screws to facilitate handling this copper ring. The mass of the copper ring was kept small to minimize its thermal capacity which in turn resulted in a greater temperature change for a given amount of added energy, and decreased the time constant of the system. The surface of the ring on which the foil was mounted was highly polished so that the foil would adhere to the ring to give good thermal and electrical contact between the foil and ring. The ring was made of copper because of the good thermal conductivity of this metal.

The copper ring fitted into a plastic ring holder. A slight trace of vacuum grease was used on the outside surface of the copper ring to hold it in the plastic ring holder.

The dimensions and hence the thermal capacity of the ring holder were kept to a minimum. The ring holder had twelve, size 80, equally-spaced holes drilled through it. Two sets of thermocouples -- six thermocouples per set -- had their junctions inserted into these holes. Bakelite cement was used to cement these thermocouple junctions in place and to provide thermal contact between the junctions and the ring holder. The ring holder was made of plastic to provide electrical insulation between the foil and the thermal junctions as well as between the junctions themselves.

b. Thermocouples and Heat Sink

The thermocouples were made of number 40 copper and number 38 constantan wires. These small wire sizes were used in order to minimize the heat losses by conduction from the foil. Copper-constantan thermocouples were used because of the relatively high thermoelectric power, tensile strength, and malleability. The tensile strength and malleability qualities were desired because the thermocouples served the mechanical function of holding the foil holder in position.

One junction of each thermocouple was inserted into a small hole in the ring holder and cemented in place with bakelite cement. These junctions were welded as follows. The ends of a copper and a constantan wire were twisted together just enough to give mechanical contact. This twisted end was connected electrically to one side of an 18 volt, 60 cycle, AC supply and inserted through a small glass tube into a bottle which had a pool of mercury in its bottom. This pool of mercury was connected electrically to the other side of the 18 volts, 60 cycle, AC supply. A continuous flow of helium filled the remaining volume of the bottle. The twisted copper and constantan junction was slowly brought into contact with the mercury causing an electric arc which welded the two wires together. The welded junction formed in this manner was a small spherical joint about 0.010 inch in diameter.

Shown in Figure (6) is the apparatus used for making the welded junctions. The bottle was a 20 ml beaker which was stoppered with a two-hold rubber stopper. Two glass tubes through the rubber stopper served an inlet and outlet for the helium gas. The latter glass tube was also used as the place for inserting the thermocouple wires to be welded. A Variac connected to a 110 volt 60 cycle AC line was used to supply the 18 volts 60 cycle AC. The rate of helium gas flow was set at about 0.1 C.F.H. as measured with a Fisher and Porter Company "Flowrator", Model 132-6.

The other end of the copper and constantan wires served as the reference junction. This junction was a pressure junction which was formed by crossing the two wires over and by squeezing them together between the two halves of a heat sink. There were twelve such junctions sandwiched in the heat sink. Screws were used to squeeze the two halves of the heat sink together.

Shown in Figure (7) is the manner in which these junctions were made. On either side of each junction was a 0.005 inch thick sheet of copper. Hence there were twelve pairs of these copper sheets. Each pair was separated from neighboring pairs so that the thermocouple junctions would not be shorted. The sheets of copper were sandwiched between two thin annular discs of teflon which in turn were sandwiched between the halves of the heat sink. The copper sheets provided a large area of contact and hence good thermal conductivity between the reference thermocouple junctions and the heat sink. The teflon sheets provided

UNCLASSIFIED
ORNL-LR-DWG. 37727

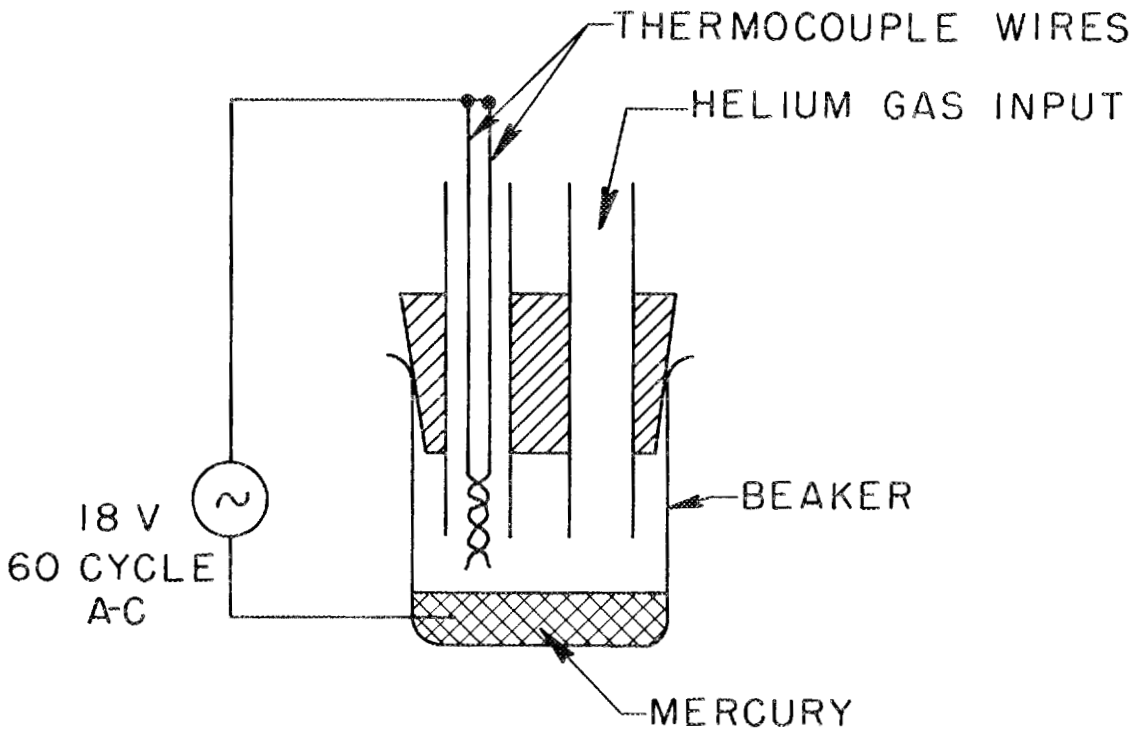

Figure 6. Apparatus for Making Welded Thermocouple Junctions.

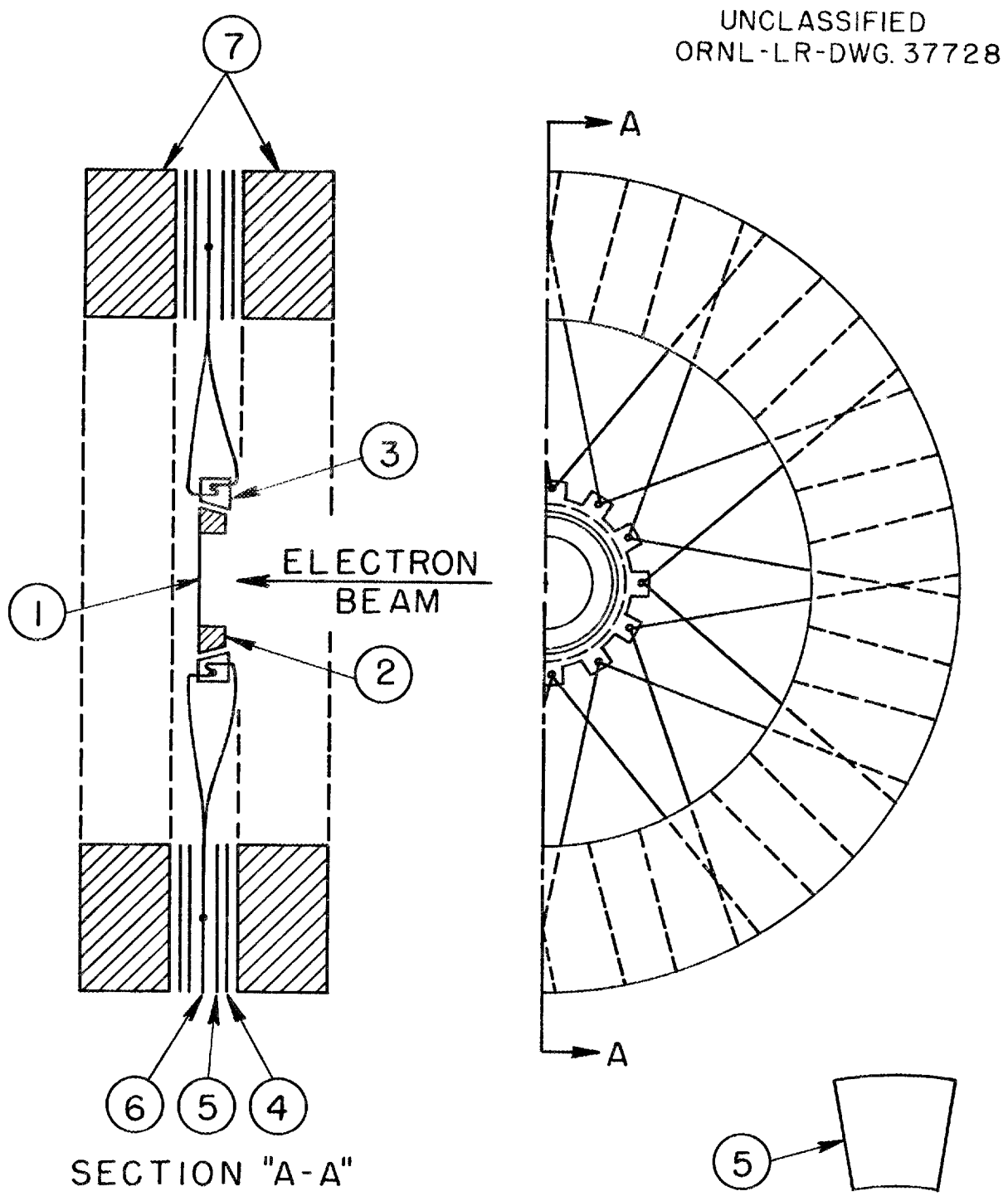

Figure 7. Assembly Drawing of the Thermocouples, Heat Sink and Foil Mount.

Parts List for Figure 7

Item No.	Description
1.	Foil
2.	Copper Ring
3.	Plastic Ring Holder
4.	Teflon Insulator
5.	Copper Plate
6.	Thermocouple Wires
7.	Aluminum Heat Sink, 4-1/2 inch O.D., 2-1/2 inch I.D., and 11/16 inch thick per each part

electrical insulation to prevent shorting out the thermocouples. The teflon sheets were made as thin as possible to improve the heat flow between the thermocouple junctions and the heat sink. The minimum thickness of the teflon sheets was limited by the protusion produced by the crossed thermocouple wires which could have pushed through the teflon sheets and shorted out the thermocouples to the aluminum heat sink had the sheets been too thin.

The heat sink was made as large as possible and made from aluminum to provide the maximal thermal capacity in a minimal mass. Since aluminum oxide is such a relatively poor electrical and thermal conductor, the heat sink was gold plated.

It may be seen in Figure (7) that the electron beam was incident on the foil from such a direction that the electrons scattered in the forward direction could not strike the copper rings. Although some of the back-scattered electrons could conceivably strike the copper ring, they were a very small fraction of the scattered electrons for a low Z material like Al in the thicknesses employed here. Had the scattered electrons been permitted to strike the copper ring, they would have dissipated most or all of their energy there and the system would have been heated erroneously.

As pointed out earlier, there were two sets of six thermocouples connected in series. One set was used for cooling the foil by means of Peltier cooling. The other identical set was used for monitoring the

foil temperature. Shown in Figure (8) is an electrical diagram of the thermocouple circuits. For convenience, only one of the six thermocouples in each set is shown in this drawing. The function of switch S3 is to permit reversing the direction of current flow (i_4) through the cooling thermopile so that the foil may be conveniently heated or cooled by the Peltier effect. As is well known these effects are exactly reversible. When a current flows through a thermocouple junction, the heat generated by the junction or the heat absorbed by the junction from its surroundings is just equal to the product of its thermoelectric power, its absolute temperature, and the current flowing through it.

There were several reasons for having six thermocouples in each thermopile. It was considered desirable in the case of the cooling thermopile to cool the foil uniformly around its periphery rather than at one or a few selected points. In the case of the temperature monitoring thermopile, it was considered desirable to monitor the foil temperature at several points around its periphery. The reason for this is that the diffuse electron beam may have "hot spots" in it which would heat the foil more at some points than at others. In addition, the large number of thermocouples gave more sensitivity to temperature. After the experiment was concluded, it was felt that undue emphasis might have been placed on this consideration, and that a thinner ring of lower heat capacity and with only one measuring and one cooling thermocouple would have been better. This is discussed in the Conclusion section.

UNCLASSIFIED
ORNL-LR-DWG. 37729

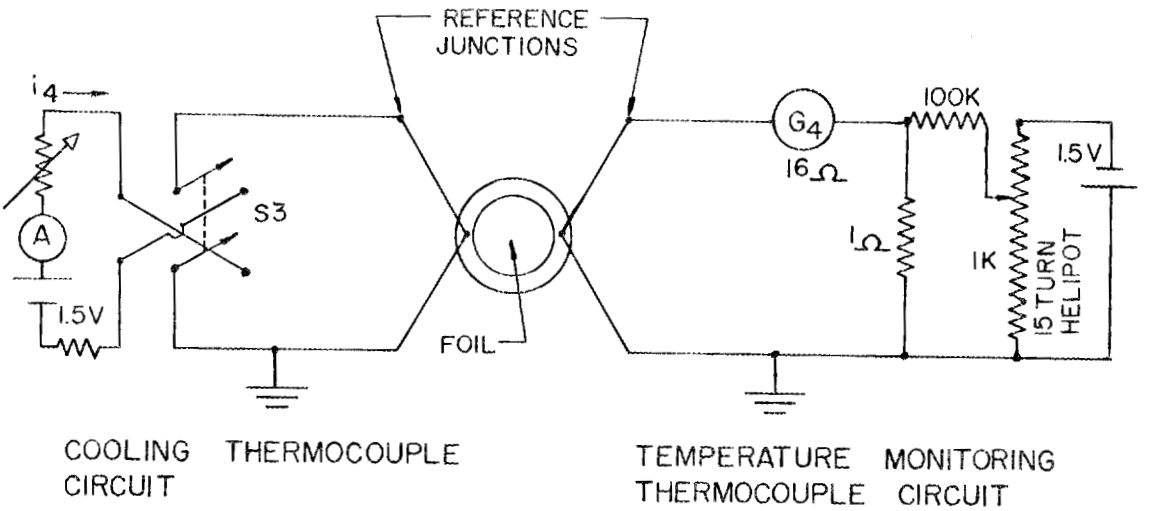

Figure 8. Thermocouple Circuits.

The ammeter for measuring the cooling current i_4 was a Weston DC ammeter, model 45 and had an external shunt. With the external shunt provided it gave a full scale reading at 10 ma. It had an accuracy of $\pm$ 0.25% of full scale, and the shunt was accurate to within 0.1%. The cooling current was controlled by a variable resistance in series with the cooling thermopile. A fixed resistor in series with the variable resistance was used to limit the cooling current and protect the ammeter. The cooling current could be turned off and on and reversed with switch S3.

The galvanometer G4 measured the thermal e.m.f. of the temperature monitoring thermopile. This was a Leeds and Northrup galvanometer (Y-84951) which used an external scale. It had a focal distance of 91 cm, and a sensitivity of 0.074 microvolts per millimeter deflection. Since the thermoelectric power of a copper-constantan thermocouple is about 40 microvolts per centigrade degree, the sensitivity of this thermopile was about six times forty divided by 0.074, or about 3160 millimeters per centigrade degree.

Galvanometer G4 called for a critical damping resistance of 17 Ω. It had an internal resistance of 15.6 Ω, and a period of 4.8 seconds. The thermopile had a resistance of about 16 and served as the critical damping resistance. Shown in Figure (9) is a potentiometer type circuit which was used to provide an e.m.f. for zeroing the galvanometer. The galvanometer itself was mounted on a one foot square steel slab four inches thick which fitted into a 15 inch cubic wooden box which had been filled with foam rubber.

UNCLASSIFIED
ORNL-LR-DWG. 37730

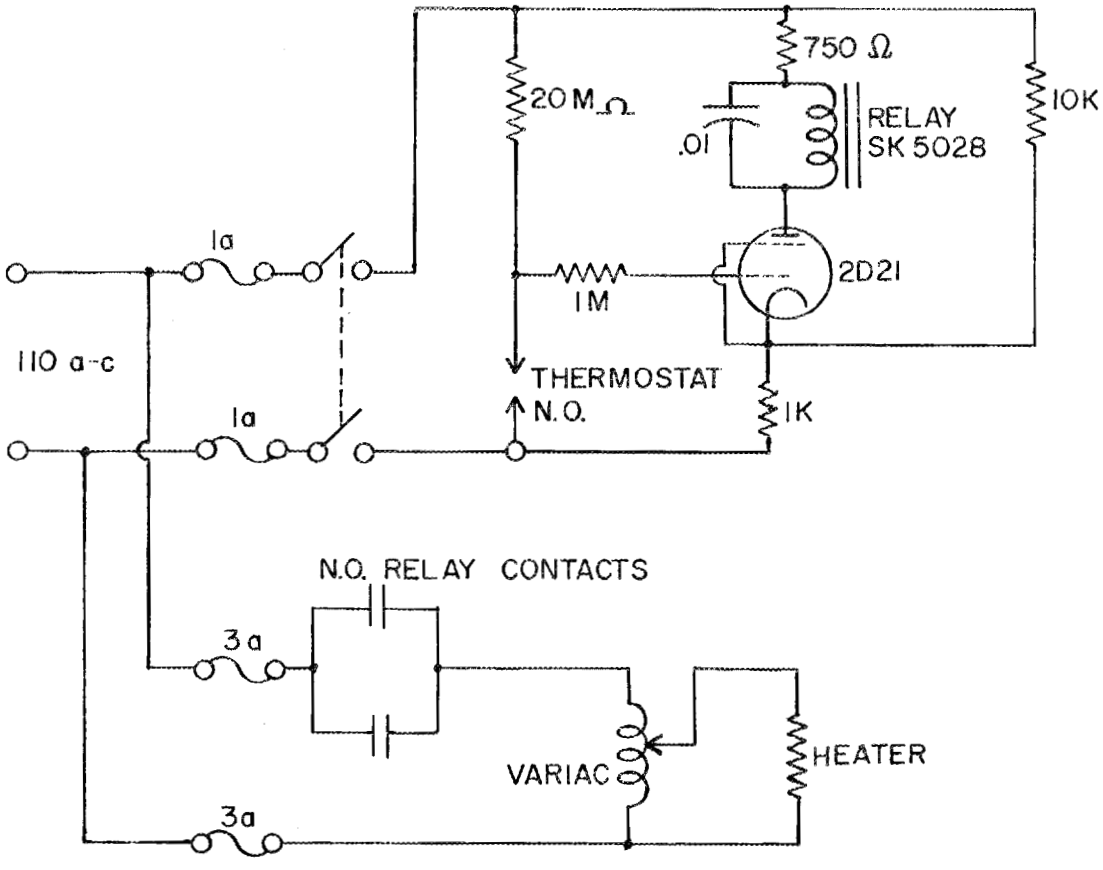

Figure 9. Control Circuit for Constant Temperature Furnace.

For monitoring the rate of drift of the foil temperature, a 10 r.p.m. Bodine motor was used to close a microswitch every revolution. The microswitch momentarily energized a buzzer to give a noise signal every 0.1 minute. The readings of galvanometer G4 were recorded manually at each of these signals.

c. Isothermal Furnace and Temperature Control

It was necessary to control the environmental temperature of the heat sink to within very close tolerances because of the high sensitivity of the temperature monitoring thermopile. The apparatus for measuring $\overline{\Delta E}$ was placed in an aluminum cylinder equipped with flange for bolting it in place at the end of the accelerator. This aluminum cylinder was 6-1/2 inches in diameter on the inside with a 1/16 inch wall thickness. Asbestos tape was wound around this cylinder to provide a one-inch-thick layer of insulation. Then a 12-inch diameter copper cylinder was placed around this aluminum cylinder and concentric with it, thus providing an air space for more insulation between the two cylinders. The outer cylinder was made of 1/16-inch-thick copper to provide good heat conduction throughout its length.

The outer cylinder was heated to a constant temperature. This was done by wrapping around this cylinder a 40-foot long, 400-watt, 110 AC heating wire of the type used in homes for radiant heat in the ceiling. Over and around the wire and outer cylinder was placed a layer of furnace cement which was about 3/8-inch thick. A hole was

drilled through the outer cylinder and a stainless steel tube was placed through this hole at such an angle that three inches of this tube extended down into the air space between the two cylinders. This stainless steel tube, sealed at the bottom, was silver-soldered to the outer cylinder to provide good heat conduction to it. The tube was filled with mercury and a mercury-to-wire thermostat having a sensitivity of 0.01 degrees centigrade was then placed into it.

The inside diameter of the tube was only about 0.010 inches larger than the diameter of the sensitive part of the thermostat in order to provide maximum thermal conductivity through the mercury to the thermostat. The tube was deep enough so that the sensitive part of the thermostat extended all the way down into the air gap between the two cylinders, where the temperature was expected to be more stable than the outside temperature. The tube was made of stainless steel because it does not amalgamate with mercury as readily as do other materials.

The thermostat controlled the power input to the heater. The control circuit is shown in Figure (9) which was used. This control circuit was designed by J. A. Harter in the Health Physics Division of the Oak Ridge National Laboratory and operated as follows. With the thermostat normally open, the values and phase relationship of the plate and grid potentials are such that the 2D21 tube conducts on the positive half-cycle. This energizes the relay in the plate

circuit, closing the normally open relay contacts. This applies power to the heater by way of a Variac. When the temperature increases, the thermostat contact closes, shutting off the 2D21. The relay de-energizes, and its contacts open disconnecting the power to the heater until the system cools, and the cycle is repeated.

The thermostat was adjusted to hold the heater temperature at about 29 degrees centigrade, independently of the ambient room temperature. The room was air conditioned and its temperature was thermostatically controlled to within 3 degrees centigrade. The Variac output to the heater was adjusted so that the heater on and off times were equal to give optimum temperature control. Although the thermostat could respond to a change of 0.01 degrees centigrade, the heater temperature oscillated approximately 0.1 degrees centigrade above and below its average temperature. These temperature oscillations were considerably damped out at the heat sink of the temperature monitoring thermopile because of the large thickness of the air, asbestos, and vacuum heat insulation between the heater and heat sink.

It should be pointed out that the end of the heater was covered with a thin aluminum plate which was lined on the inner side with a 1/8-inch-thick layer of asbestos. Between this plate at the end of the heater and the end of the inner cylinder, which housed the apparatus, was about a 1-1/2 inch air gap. At the end of the inner cylinder was a 3/4-inch-thick lucite plate with an O-ring seal to provide a vacuum seal.

Two holes with O-ring seals were provided in this lucite plate. One hole was for an ionization pressure gauge which measured the pressure at this point in the system. The other hole was for a specially built brass tube, which had a "Kovar" seal and Amphenol connectors for the wire connections to the apparatus.

C. The Determination of $\overline{\Delta X}$

A modified "Cahn Electrobalance", model M10, made by the Cahn Instrument Company, Downey, California, was used for weighing a known area of foil. The unmodified electrobalance will first be described and then the modifications and the improvement each made will be given.

1. The Cahn Electrobalance

Shown in Figure (10) is a schematic of the commercial electrobalance. The torque motor drives a lever or balance arm on which a stirrup and pan are mounted. This pan holds the object to be weighed. The balance resistor R9 is used to vary the current through the torque motor to bring the lever arm to a fiducial mark. This position is attained when the shadow of the balance arm cast by a light beam is directly in line with a segmented fiducial mark scribed on a frosted glass screen. Figure (11) is a drawing of the electrobalance weighing mechanism.

UNCLASSIFIED
ORNL-LR-DWG. 37731

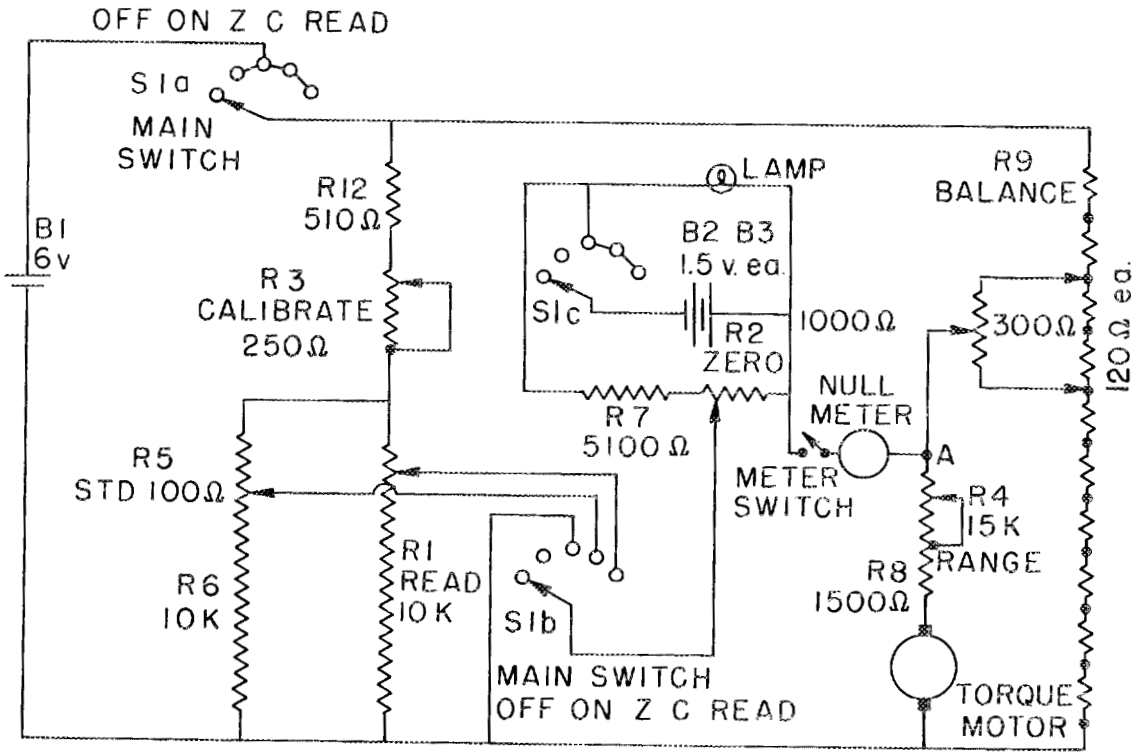

Figure 10. Schematic of Cahn Electrobalance Model M-10.

UNCLASSIFIED
ORNL-LR-DWG. 37732

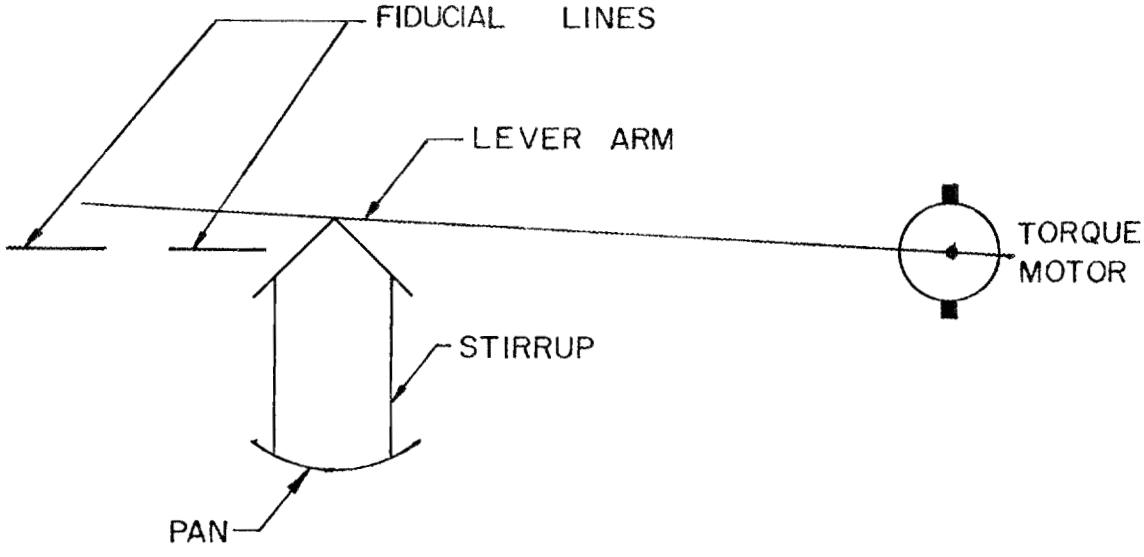

Figure 11. Electrobalance, Pan, Arm, and Torque Motor.

As can be seen in Figure (10), the potential drop across R4, R8, and the torque motor was measured with a potentiometer type circuit. The resistor R4 was a range resistor which determined the magnitude of this potential drop for a given weight range. The variable resistor R2 with the batteries B2 and B3 was used to "buck out" the potential necessary to balance the empty pan. Hence, R2 was labelled as the zero control. The variable resistor R3 was used when a calibrated weight was in the pan so that the Duo-dial setting of the helipot R1 would give a direct reading of the weight in the pan.

The accuracy of the electrobalance was determined by several factors. The Duo-dial on the helipot had 1000 divisions, and by interpolation between the divisions the Duo-dial could be read to about two parts in 10,000 at full scale. As designed, the minimum range for which the electrobalance could be calibrated was five milligrams. The linearity of the helipot R1 was 0.05%, which corresponds to an error of $\pm$ 2-1/2 micrograms on the 5 milligram range. If all possible sources of error are considered and the overall error calculated by taking the square root of the sum of the squares of the errors, an overall error of about $\pm$ 8 micrograms is obtained for the 5 milligram range. Since foils having thicknesses of the order of 100 micrograms per square centimeter or less were to be studied, this accuracy was not considered good enough. Hence, several modifications were incorporated into the electrobalance.

In balancing the lever arm by lining it up with the fiducial lines, one could obtain greater reproducibility by approaching the fiducial line consistently from the same direction. In this work, the fiducial line was approached from the bottom.

2. Modifications to the Electrobalance

Several modifications were incorporated into the electrobalance. The effect of each successive modification on the accuracy of the microbalance was ascertained.

First, the six volt dry cell B1 was replaced with a 6 volt wet cell and all variable resistors were replaced with 10 turn helipots to give a more stable e.m.f. source and more vernier control, respectively. National Bureau of Standards, class S, calibrated weights of 1, 2, and 3 milligrams were weighed on the 5 milligram range which was calibrated with a 5 milligram, National Bureau of Standards, class M, weight. The readings were not very reproducible, particularly for the 1 milligram weight, where the maximum deviation between successive readings was 7 micrograms. The standard error was 0.26%. It was concluded that these modifications did not improve the accuracy of the electrobalance very much. This implied that the inaccuracy was due to a large extent to the errors inherent in the potentiometer circuit for measuring the potential drop across R_4, R_8, and the torque motor.

A type K-2 Leeds and Northrup potentiometer was then used to measure the potential drop across the torque motor for successive readings using the 1 milligram weight. With this potentiometer the potential drop across the torque motor, which was of the order of 22 millivolts, was measured to within a few microvolts. The reproducibility for successive readings was not very good. Hence, the resistor R8, which was a $\pm$ 20% carbon, fixed resistor, was replaced with a 1000, $\pm$ 0.5%, nichrome, wire-wound resistor. The K-2 potentiometer was then used to measure the potential drop across this resistor. Using this method, the standard error for ten successive measurements was 0.083%, for the 1 milligram weight.

To improve the accuracy further, a microscope having a magnification of 16, and made by the Central Scientific Company, was used to improve the optical system. With this the lever arm could be brought to the balance position in line with the fiducial lines more accurately. The standard error was only 0.056% when the 1 milligram weight was weighed ten times.

In order to minimize errors resulting from friction in the torque motor bearings, a small amount of alternating current was applied to the torque motor. This was done by applying the 110 volt, AC line through current limiting resistors and condensers on each side of the AC line and thence to the torque motor. The condensers were used to block the DC of the electrobalance. The values of resistance and capacitance were varied until the 60 cycle vibration

of lever arm was barely discernible. The ultimate values were 43KΩ and 0.1 μf on each side of the AC line leading to the torque motor. A two pole on-off switch and headphone plug were used to be sure that this AC vibration was on only when measurements were made in order to prevent excessive wear on the torque motor bearings. Using this additional improvement, a 1 milligram weight was weighed 10 times. The standard error was reduced to 0.011%.

Table I gives the modifications and the effect each successive modification had on the accuracy of the electrobalance. The errors are tabulated as absolute errors rather than percentage errors because the absolute error seemed to remain fixed when the 1, 2, and 3 milligram standard weights were weighed. This implies that the absolute error may be about the same for smaller weights.

D. Preparation of Foils

Two methods for making thin uniform foils were employed which differ only slightly from the methods described in the literature[21,22]. In one method, a carefully cleaned glass slide was first dipped into a solution containing 0.1 grams of Formvar dissolved in 9 milliliters of ethylene dichloride to which 50 drops of methyl alcohol had been added. One of the most successful methods found for cleaning the glass slides was to rub them clean with either "Bioloid" number 17471 lens paper or "Sight Savers" a Dow Corning silicone treated tissue. The Formvar used was a 15/19 resin produced by the Shawinigan Products Corporation,

[21] S. D. Warshaw, Rev. Sci. Inst. 20, 623 (1940).

[22] W. Franzen and L. Schellenberg, Rev. Sci. Inst. 27, 171 (1956).

TABLE I

Electrobalance Modifications and the Resulting Improvement

(Using a 1 mg. Weight)

	Modification	Absolute Standard Error in μg
1.	None	5
2.	Dry cell replaced by wet cell, and variable resistors replaced by 10 turn helipots.	2.6
3.	K-2 potentiometer used to measure potential drop across precision resistor in series with motor.	0.84
4.	Microscope having a magnification of 16 used to magnify the fiducial lines.	0.56
5.	AC vibration used to reduce frictional errors.	0.11

New York City. After dipping, the glass slides were hung up to dry in an air-conditioned room. The slides prepared in this manner were used in the preparation of the aluminum foils used in this experiment.

The evaporator was a glass bell jar pumped down with a large Duo-Seal Forepump and a oil VMF 260 diffusion vacuum pump. After pumping down to about 0.15×10^{-5} millimeters of mercury, liquid nitrogen was added to the cold trap to bring the pressure down to about 10^{-6} millimeters of mercury. The glass slides were mounted beforehand in the evaporator at distances of 10.6, 15, and 21.2 centimeters from the filament used for evaporating the aluminum. Aluminum wire bent in the form of a horseshoe was hung on the center of the filament where a small "U" was formed to hold the aluminum. The filament was made of number 40 tantalum wire. The mass of aluminum wire to be evaporated was 283 milligrams.

A Variac was used as the power supply for the filament. The Variac output was slowly increased until visual observation showed that the aluminum wire melted to form a bead in the U-shaped center of the filament. The aluminum bead then wetted the filament. Again the Variac output was slowly increased further until the aluminum evaporated off the filament. This complete operation took about two minutes.

For the distances (d) at which the glass slides were mounted from the point source of aluminum, foil thicknesses of close to 200,100 and 50 micrograms per square centimeter were evaporated onto the slides. This is in accordance with the inverse square low

$$t = \frac{m}{4\pi d^2}$$

where t is the foil thickness in milligrams per square centimeter, m is the mass of metal evaporated in milligrams, and the distance d is in centimeters.

The foil on the glass slide was cut into 3/4 inch squares by scribing through it with a razor blade. The copper ring foil holders were cemented onto these areas with India ink which served as both an electrical conductor and a binder. After the India ink had dried, the glass slides with the foil and copper rings were immersed into ethylene dichloride to dissolve theFormvar film between the metal foil and the slide. The mounted foils were then slowly slid off the glass slide and then lifted in a vertical plane out of the ethylene dichloride so that surface tension would not break the foil. Several, smooth, 50, 100, and 200 micrograms per square centimeter aluminum foils were successfully mounted in this manner.

A somewhat better method was suggested by J. V. Cathcart and J. Campbell of the Metallurgy Division at the Oak Ridge National Laboratory. In this method glass slides were cleaned as before. In this case, the glass slides were number 14340-A, non-corrosive, select grade, size 3 × 1 inches, "Micro-Slides" made by the W. H. Curtin Company, New Orleans, Louisiana. These slides were highly polished and had smooth ground edges which proved to be advantageous.

The slides were mounted in the evaporator at a distance of at least 10 centimeters from the metal to be evaporated in order to get uniform foils. Two separate filaments were used. One filament was used to evaporate some Victawet onto the glass slide before evaporating the metal. Victawet is a wetting agent made by the Vicks Chemical Corporation. The filament for evaporating the Victawet was a 0.015 inch diameter tungsten filament which was wound in the central region to form a conical cup for holding the Victawet. Using the same evaporation and pressures already described, the output of a Variac was slowly increased to give 16 volts across this filament. The Victawet was then allowed to evaporate slowly. This caused the pressure to go up. The pressure was then allowed to come down again to about 0.15×10^{-5} millimeters of mercury before evaporating the metal.

Several different metal foils were evaporated onto slides prepared in the above manner. Although these foils were not used in stopping power measurements, the techniques used in their preparation will be

included for completeness. Different techniques had to be employed for each metal in the evaporation process. For example, silver was evaporated by placing it on a 0.003 inch thick by 0.25 inch wide tantalum ribbon filament. The filament was curled up a bit on its edges to hold the molten silver during the evaporation process. This was done because silver would not wet the filament and would otherwise drop off before it would evaporate.

To evaporate chromium, it was found necessary to electroplate it first onto a helical tungsten filament. First, oxidized lead was prepared by using lead at the anode and graphite at the cathode in a 2 molar sulfuric acid solution. The power source was a Mallory battery charger, type 107 made by the P. R. Mallory Co., Inc., Indianapolis, Indiana. The current was controlled with a rheostat to be about 2.5 amperes for this oxidation process which lasted for about eight minutes. Then to electroplate the tungsten filament with chromium, the tungsten filament was used as the cathode with the oxidized lead as the anode in a solution made of 40 grams of chromic acid (solid), 0.4 milliliters of concentrated sulfuric acid, and 160 milliliters of water. Oxidized lead was used as the anode because it gave the best results. When lead was used as the anode, an insulating layer of lead chromate formed on the lead causing the current to decrease gradually. When graphite was used as the anode, the graphite disappeared into the solution, causing the electroplating current to

decrease gradually. The Mallory Battery charger was again used as the electrical power source. The current was controlled with a rheostat to about 2 amperes for about 20 minutes to give a current density at the cathode of 80 amperes per square centimeter of cathode surface.

In the evaporation process for chromium, the Variac output to the electroplated filament was slowly increased with the pressure being observed continuously. Initially the pressure went up quickly to about 10^{-4} millimeters of mercury. Time was allowed (one to two minutes) for the pressure to come back down to about 0.15×10^{-5} millimeters of mercury. The Variac output to the filament was then increased further until the pressure went up to 0.2×10^{-5} millimeters of mercury. Actually the chromium does not evaporate, because of the oxide coating which forms on it; rather, the chromium sublimes. In about five minutes or more, enough chromium sublimed to give a good film on the glass slide. Usually two or more glass slides were used in one operation to improve the chances of getting a good foil mounted on the copper ring holder.

An excellent reference on the evaporation techniques of thin films is the recently published book by Holland[23].

After the metal film was evaporated onto the glass slide, the liquid nitrogen was removed from the cold trap of the evaporator.

---

[23] L. Holland, VACUUM DEPOSITION OF THIN FILMS, (Chapman and Hall Ltd., London, 1956).

The cold trap was warmed up by compressed air blown on it with an air hose. The diffusion pump was then turned off and cooled off with the air hose. Then the forepump was turned off. Air was let into the system through silica gel to absorb the moisture in the air before it was admitted to the system. The glass slides were removed from the evaporator and placed in Petri dishes to keep the metal film free from dust.

To remove the foil from glass slide, the following procedure was used. The edges of the glass slide were scraped with a knife to facilitate peeling the foil off. The foil was peeled off the glass slide by sliding the glass slide into some warm tap water at a 45° angle. This was done very slowly and with a steady hand to keep the foil from tearing. The water dissolved the wetting agent and the surface tension peeled the foil off. The foil floated on the surface of the water.

To get the foil mounted, some detergent was first dissolved in some warm tap water in a separate beaker. A small amount of this solution was poured into the water holding the foil, to decrease the surface tension of the water. The copper ring was then brought under the foil and a piece of the foil draped over the copper ring was lifted vertically out of the water. It should be pointed out that the surface of the copper ring on which the foil was mounted was first highly polished on a gem polishing machine. A fine abrasive, type B-5125

made by Linde Air Products Company, New York City, was used. This was done so that the foil would adhere to the copper ring.

Another method for getting the foil out of the water and onto the copper ring was also used. A brass sheet about 2 inches square and 1/32-inch thick had a 3/4 inch hold punched in the center. A handle was soldered onto this sheet for holding it. An 0-80 brass screw was put into one of the tapped holes of the copper ring. The head of this brass screw was glued to this brass sheet in such a manner that the copper ring was concentric to the hole in the brass sheet and its face flush with one surface. "Duco" cement was used to glue the screw to the sheet. The sheet and ring were used to lift the foil from the water vertically so that the foil draped over the hole and copper ring. After drying, the foil was trimmed around the edges of the hole and the residue was folded over the copper ring. Acetone was used to dissolve the "Duco" cement, and the copper ring with the mounted foil was removed from the brass sheet.

This latter method proved to be the more successful method for mounting the thinner foils. Self-supporting foils thin enough to see through were successfully mounted in this manner. However, these thinner foils were too fragile to be transported to the accelerator and put in place. It is believed that had the copper ring been smaller in diameter, these thinner foils would have been much stronger.

VI. PROCEDURE

The stopping power is the ratio of the average energy loss $\overline{\Delta E}$ to the average path length $\overline{\ell}$ of the electron as it goes through the foil. This average path length $\overline{\ell}$ is the sum of the average foil thickness $\overline{\Delta x}$ and the average increase in path length $\overline{\Delta \ell}$ resulting from multiple scattering within the foil. The procedure was to measure $\overline{\Delta E}$, and $\overline{\Delta x}$, and to calculate $\overline{\Delta \ell}$ in order to obtain $\overline{\Delta E}/\overline{\ell}$.

A. Measurement of $\overline{\Delta E}$

As shown in Equation (54), the time rate of temperature change of the foil ($\dot{T}$) is given by

$$\dot{T} = K_1 \overline{\Delta E}\, i_B - K_2 (T-T_o) \quad , \tag{79}$$

where $\overline{\Delta E}$ is the average energy lost by the electrons in going through the foil, i_B is the electron beam current, T_o is the environmental temperature, K_1 and K_2 are constants of proportionality which are to be determined. The determination of $\overline{\Delta E}$ proceeds as follows.

1. Determination of K_1 and K_2

The apparatus described earlier for measuring P_B was put into the accelerator. The heater for controlling the temperature T_o was installed and the heater was turned on. The accelerator was then slowly pumped down through a small throttled orifice with the small Duo-Seal vacuum pump in order to reduce the air currents in the accelerator so as not

to break the fragile foil. After the pressure in the accelerator had reached about 100 microns of mercury, the small Duo-Seal vacuum pump was turned off. The valve to the evacuated lines to the diffusion pump and large forepump was opened. The pressure was allowed to be brought down to about 0.5×10^{-6} millimeters of mercury. The ambient temperature T_o as measured by the temperature-monitoring thermopile was noted. The galvanometer (G4) which measured the e.m.f. of this thermopile was zeroed.

The cathode-ray gun was activated as described earlier. The high voltage to the accelerator was turned off and the accelerator was grounded. The second anode potential of the cathode-ray gun then determined the electron beam energy. The electron beam was focused on the foil by varying the magnetic deguassing fields to give a maximum foil current, and a minimum aiming screen current. At these low beam energies the electrons were completely absorbed in the foil as determined by zero current to the Faraday cup.

The foil temperature determined by galvanometer G4 was measured in units of centimeters of deflection with 25 centimeters, the center of the galvanometer scale, corresponding to the ambient temperature T_o. The foil was first cooled to 15 centimeters. The electron beam was controlled manually by varying the grid potential of the cathode-ray gun to keep the beam current constant. The timer which gave a buzzing signal every 0.1 minute was turned on. The foil temperature was recorded every 0.1 minute to get the rate of the temperature drift.

This was done for various beam currents, and with beam energies low enough for the beam to be completely absorbed in the foil. Various bias disc potentials were applied also. The beam energies were varied from about 750 to 2500 volts. At these beam energies the electrons were completely absorbed in the foil so that the current measured to the foil was the beam current. The beam currents were varied from about 0.05 to 0.4 microamperes. Thus the range of beam power P_B absorbed in the foil at full absorption of the beam was from about 50 to 400 microwatts. The bias disc potential was varied from 0 to 2400 volts, in no case being larger than the beam energy used in order to permit the electrons to reach the foil. This bias disc potential did not affect the energy of the electrons striking the foil because the latter was close to ground potential at all times.

The temperature T was plotted as a function of time t for a given beam power and bias disc potential. The time t_o was defined as the time at which the temperature T was equal to T_o or 25 centimeters. The observed slope $\dot{T}$ at $T = T_o$ was determined by the method of least squares using those observed points within a time interval of 0.5 minute on either side of t_o. Shown in Figure (12) are some typical temperature-versus-time curves. Now as shown earlier in Equation (74),

$$\left[\dot{T} \right]_{T_o} \cong K_1 P_B \quad , \tag{80}$$

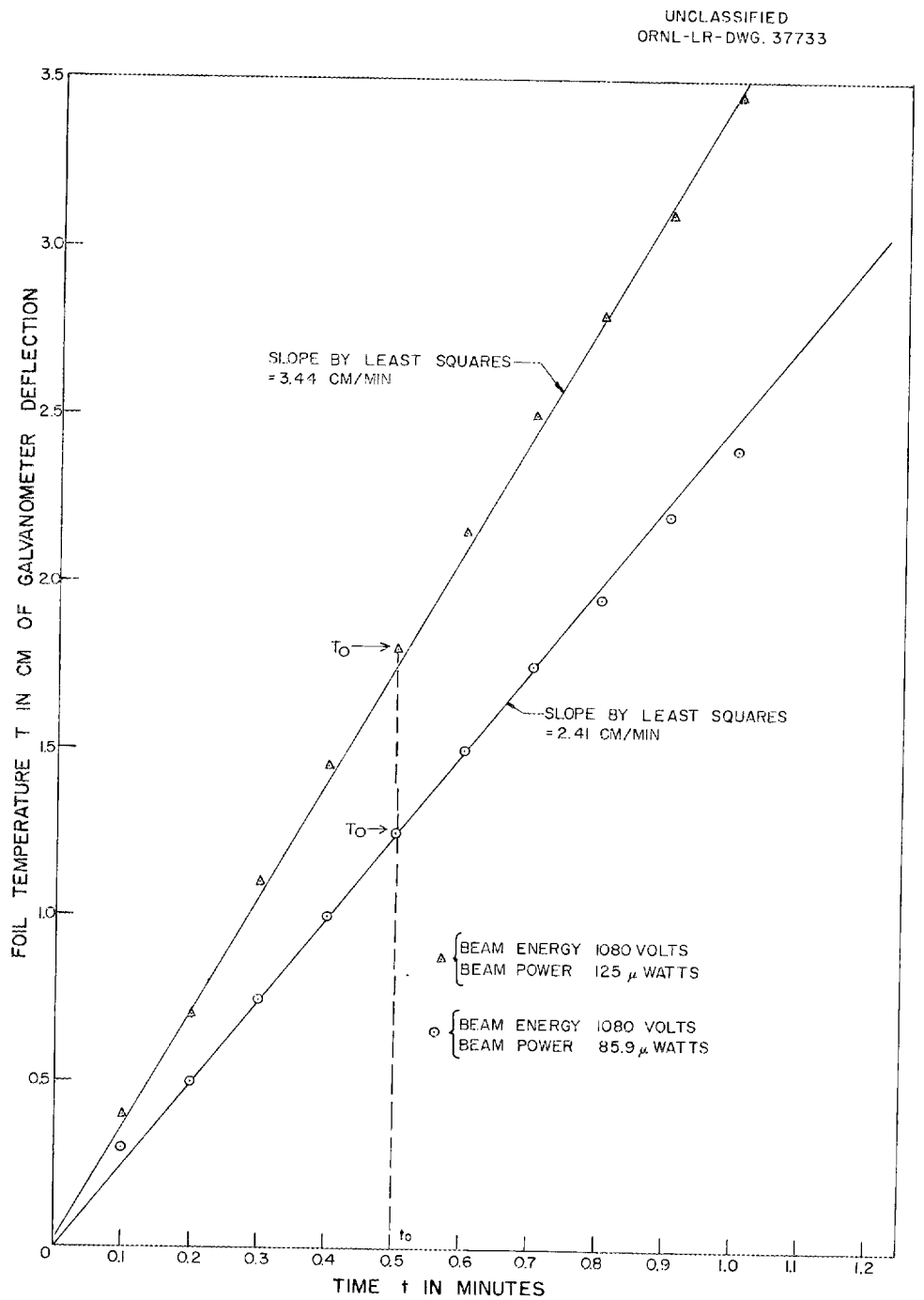

Figure 12. Typical Temperature Versus Time Curves.

when

$$(K_2 \Delta t)^2 \ll 6 \quad . \tag{81}$$

As shown in Equation (77)

$$\log_{10} \frac{T-T_o}{T_i-T_o} = -0.435\, K_2 t \qquad \text{when} \quad P_B = 0 \tag{82}$$

where T_i is the initial temperature to which the foil was cooled. Therefore, to determine K_2, the foil was precooled to $T_i = 15$ cm, and the foil was allowed to drift toward T_o. The temperature T was observed every 0.1 minute. Then the ratio $\frac{T-T_o}{T_i-T_o}$ was plotted as a function of the time t on semi-log paper, with t being plotted on the linear scale. Shown in Figure (13) is the resulting curve. From this curve it was found that $K_2 = 0.326\ \text{min}^{-1}$. Hence for $\Delta t = 0.5$ minute,

$$(K_2 \Delta t)^2 = (0.163)^2 \cong \frac{1}{36} \ll 6 \quad . \tag{83}$$

Thus it can be seen that

$$\dot{T} \cong K_1 P_B \quad . \tag{84}$$

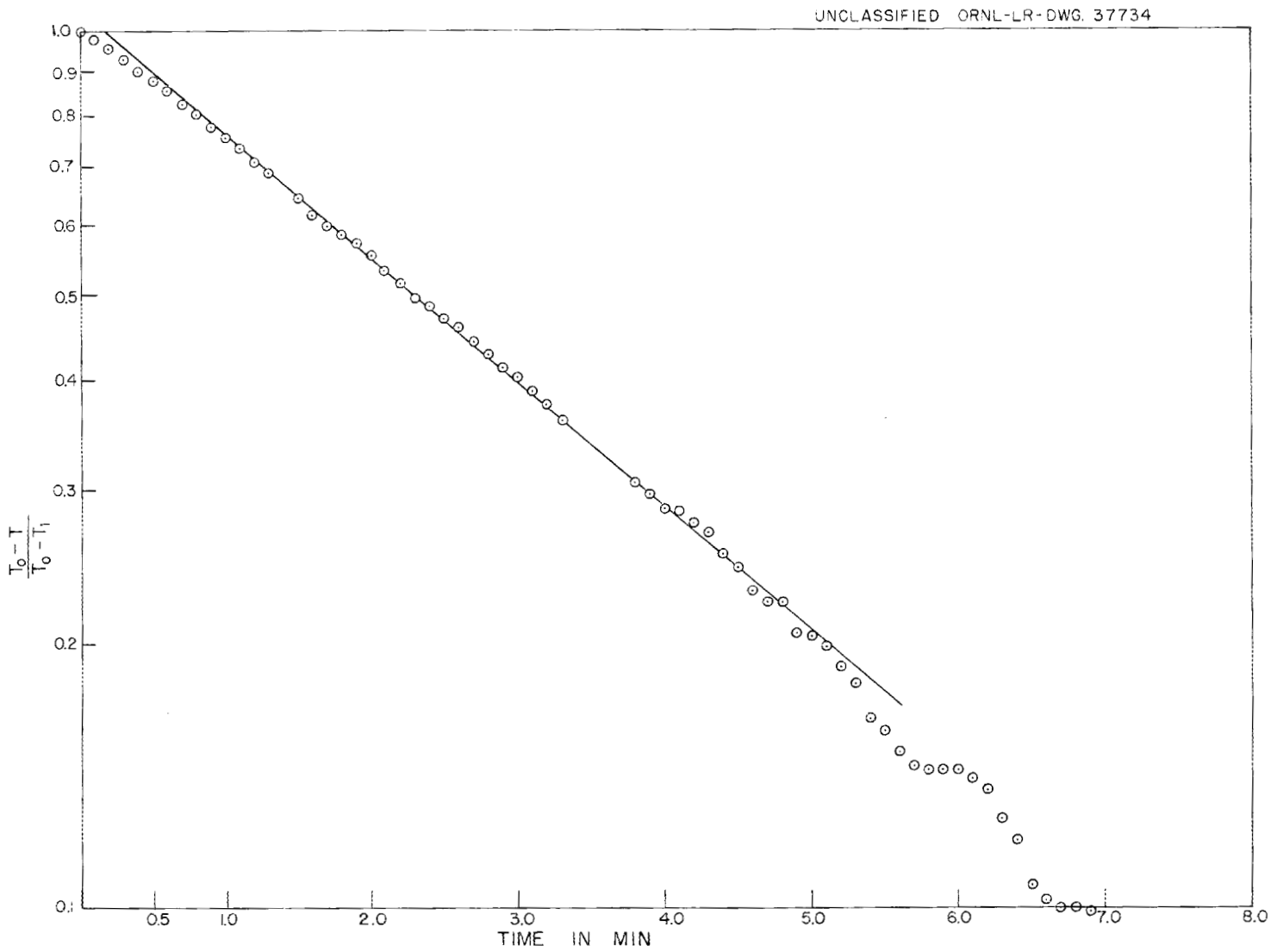

Figure 13. Logarithmic Graph of Temperature Versus Time.

It was found that the bias disc potential E_{Bias} could be varied from about -200 volts to -2400 volts without significantly affecting the calibration constant K_1. Usually E_{Bias} could not be increased to -2400 volts because of the arc-overs inside the system. Hence, the bias disc potential was usually kept at about -1000 volts. K_1 was also found to be independent of beam energy as long as the energy was low enough to provide complete absorption.

To determine K_1, the observed $\dot{T}$ was plotted as a function of the beam power absorbed at full absorption of the beam. Shown in Figure (14) is one such calibration curve. All calibration curves were linear which indicated that

$$P_B = \frac{1}{K_1} \dot{T} \quad . \tag{85}$$

To insure that the measured beam energies were accurate at full absorption, the second anode potential, as measured by the panel meter on the gun power supply, was checked with an electrostatic voltmeter which was accurate to $\pm$ 1%. The correction to the second anode panel meter reading was plotted as a function of the panel meter reading. A least squares fit to this calibration yielded the following expressions.

$$\Delta V = 0.038\ V + 7 \tag{86}$$

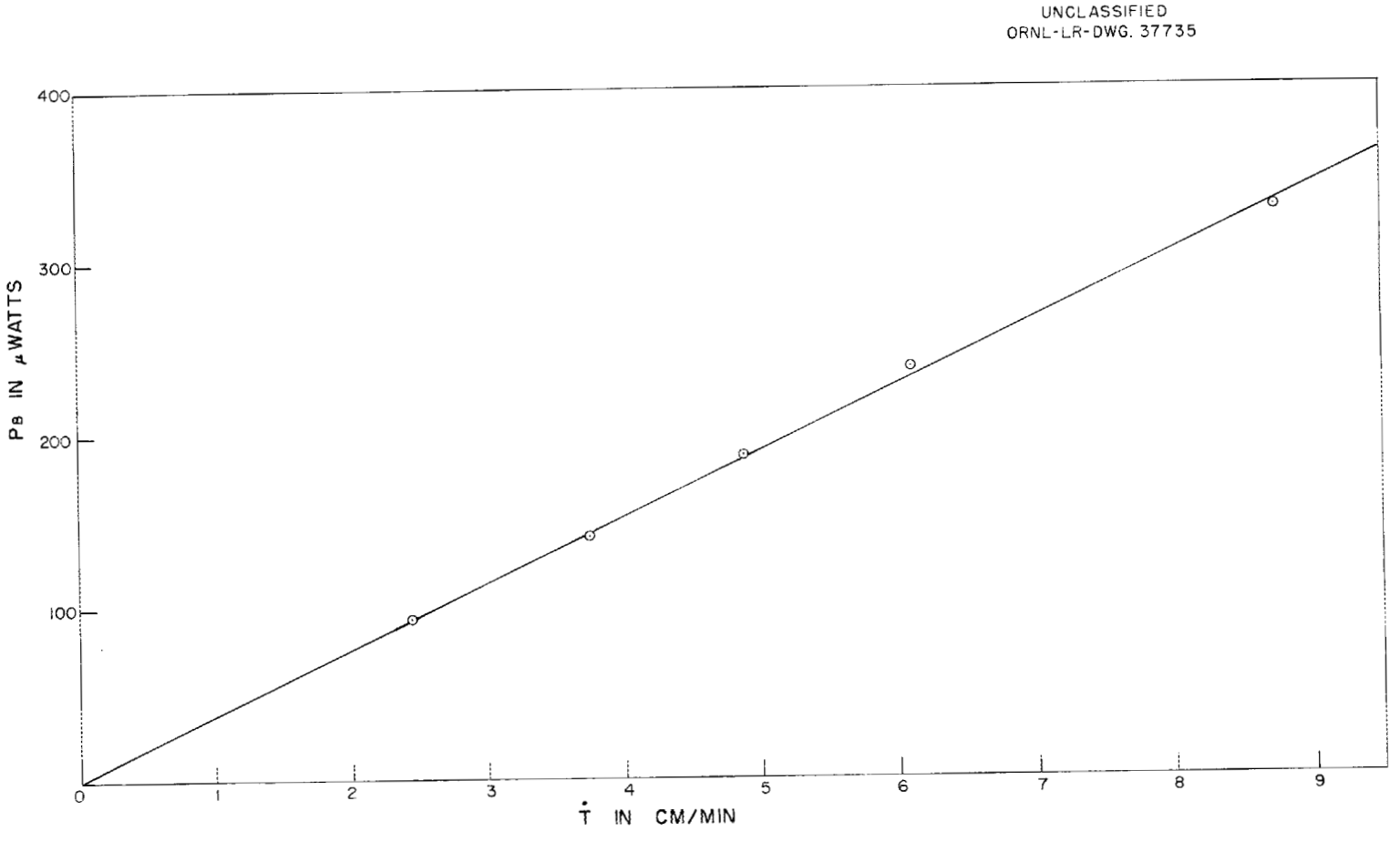

Figure 14. Calibration Curve: Rate of Temperature Change Versus Absorbed Power.

for the 0-1500 v range, and

$$\Delta V = -0.054\ V + 11 \tag{87}$$

for the 0-2500 v range. In these expressions ΔV is the correction to the panel meter reading and V is the panel meter reading.

2. Measurement of P_B

At the higher beam energies used for stopping power measurements only a small fraction of total beam power was absorbed by the foil. The accelerator potential was varied from 10 KV to 125 KV in discrete steps. The beam energy was the sum of the accelerator voltage and the potential on the second anode of the electron gun.

To check the reliability of the measurements, the beam current was varied for a given beam energy and $\dot{T}$ measured for each beam current. From each observed $\dot{T}$ and the calibration constant for the particular foil used, the power absorbed by the foil was calculated with the relationship

$$P_B = \frac{1}{K_1}\ \dot{T} \tag{88}$$

These calculated values of P_B were then plotted as a function of the beam current for the corresponding beam energy as shown in Figure (15). For each beam energy, the power absorbed can be seen to be directly proportional to the beam current.

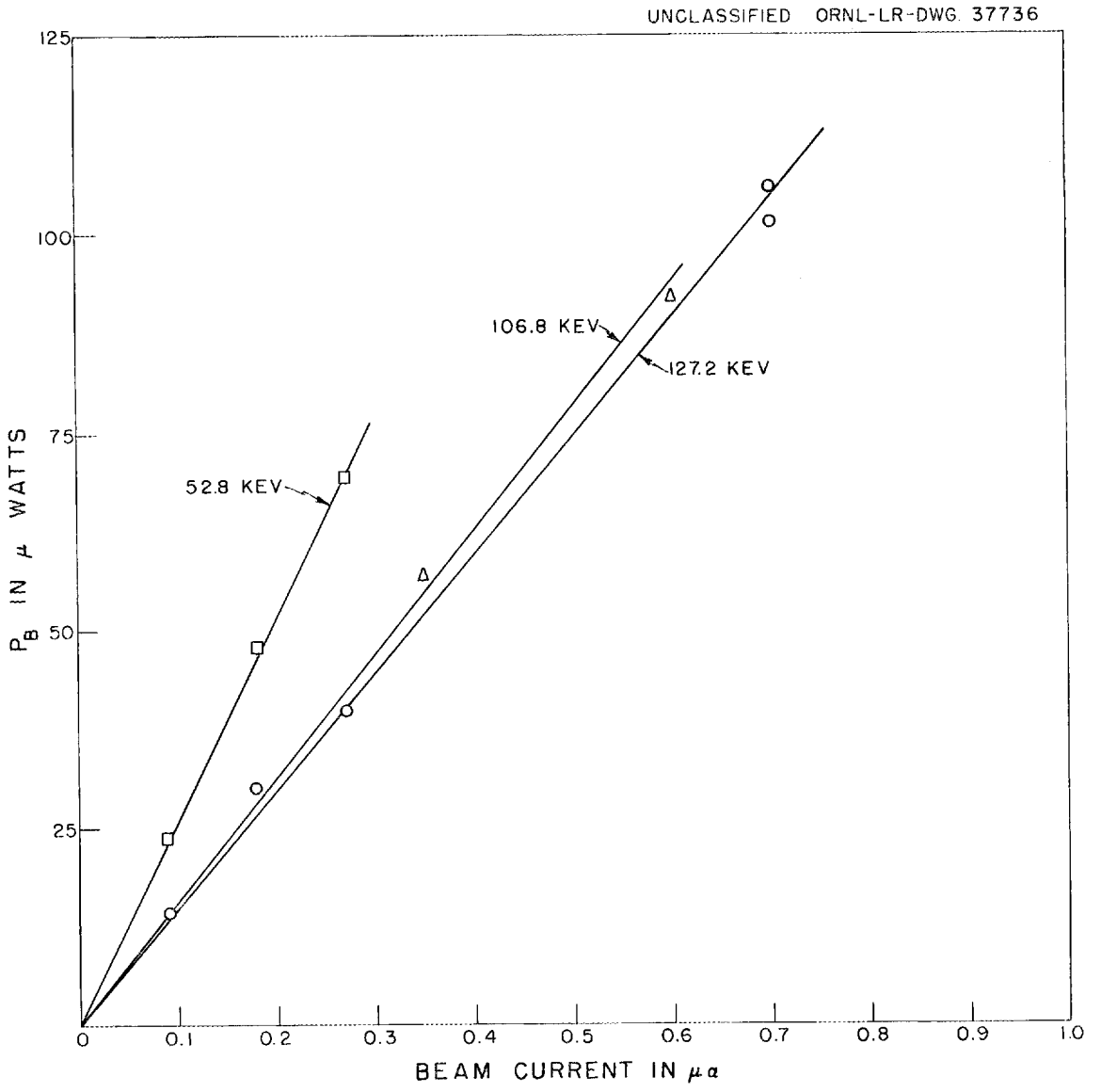

Figure 15. Absorbed Power Versus Beam Current for Various Beam Energies.

3. Determination of $\overline{\Delta E}$

As pointed out earlier, the average energy absorbed by the foil ($\overline{\Delta E}$) is given by

$$\overline{\Delta E} = \frac{P_B}{i_B} \quad . \tag{89}$$

where i_B is the electron beam current. Thus,

$$\overline{\Delta E} = \frac{\dot{T}}{K_1 \; i_B} \tag{90}$$

Electron currents to the foil and bias discs were negligibly small, and thus i_B was the Faraday cup current. The average energy lost in the foil by the electron beam was then calculated from Equation (90), using the observed values of $\dot{T}$ and beam current i_B.

Since a rough estimate of the foil thickness $\overline{\Delta x}$ was known beforehand, the ratios of $\frac{\overline{\Delta E}}{\overline{\Delta x}}$ were compared to be sure that the measurements were consistent with one another before the foil was removed from the accelerator.

B. Measurement of $\overline{\Delta x}$

To measure $\overline{\Delta x}$, the foil first had to be removed from the accelerator. To do this, the vacuum valve between the accelerator and the diffusion and forepump was closed so that the pumps could be left on. Air was slowly

let into the accelerator through a throttled air inlet after passing through a bottle of silica gel. Then the calorimeter was removed from the accelerator so that the foil mounted on the copper ring could be removed. The foil was punched out with a circular, razor-sharp punch specially made for this purpose. The diameter of the punch's cutting edge was accurately measured to be 0.442 inch, which made the area of the punched foil 0.99 cm^2. It was found that a hard, smooth surface such as a piece of formica was best for punching out the foil. A metal surface was not suitable for this purpose because the foil tended to adhere to the metal. A polished glass surface such as a glass slide was found to be suitable provided care was taken to preserve the cutting edge of the punch. It was found that the foil could not be punched on a softer surface than formica.

The punched-out foil was then weighed in the modified Cahn electrobalance, which was first calibrated with National Bureau of Standards Class M weights of 1, 2, and 3 milligrams. The balance was always calibrated before weighing a foil because the calibration could change slightly from time to time. Each standard weight was weighed ten times to improve the statistical accuracy. The 1 and 2 milligram weights were also weighed together to get a check. The weight measurement was

actually a measurement of the potential drop across a 1000 nichrome resistor placed in series with the torque motor. The weight was then given by the relationship

$$W = aV + b \quad , \tag{91}$$

where W is the weight, V is the potential measurement corresponding to the weight W, a and b are constants which were determined by a least squares fit of the calibration measurements.

The foil was then weighed alone and then with the 1 milligram standard, ten measurements being taken at each point. The foil weight was then calculated from Equation (91). The foil weight obtained by weighing the foil alone and by weighing the foil with the 1 milligram standard checked within 1 microgram. The result of the measurements then gave the foil weight to about $\pm$ 0.5 microgram. The average foil thickness $\overline{\Delta x}$ in micrograms per square centimeter was then the ratio of the foil weight in micrograms to the foil area in square centimeters.

The average increase in path length $\overline{\Delta \ell}$ of the electrons going through the foil was then calculated from Equations (36) and (50). The simpler scattering theory of Williams'[24] was used since results obtained with it did not differ much from those obtained from the more

[24] E. J. Williams, op. cit.

accurate theory of Molière[25]. Then the ratios

$$\frac{\overline{\Delta E}}{\overline{\ell}} = \langle \frac{dE}{dx} \rangle \quad , \tag{92}$$

where

$$\overline{\ell} = \overline{\Delta x} + \overline{\Delta \ell} \tag{93}$$

were calculated for each of the incident electron energies and foils used.

[25] G. Molière, op. cit.

VII. RESULTS

Shown in Figure (16) are the results of the stopping power measurements for the 50.3 and 107.8 micrograms per square centimeter aluminum foils respectively. The stopping power of the thicker foil was studied for electron energies of 12 to 102 KeV. In this run the electrons were not accelerated to higher energies because corona effects outside the accelerator became troublesome. This was subsequently remedied so that the stopping power of the thinner foil was studied for electrons having energies of 11.9 to 127 KeV. Several measurements were made for each energy using different beam currents. Probable errors were calculated for the stopping power measurements with the thicker foil. The results for both foils are shown in Figure (16) along with the Bethe stopping power theory. It may be seen that the agreement is excellent.

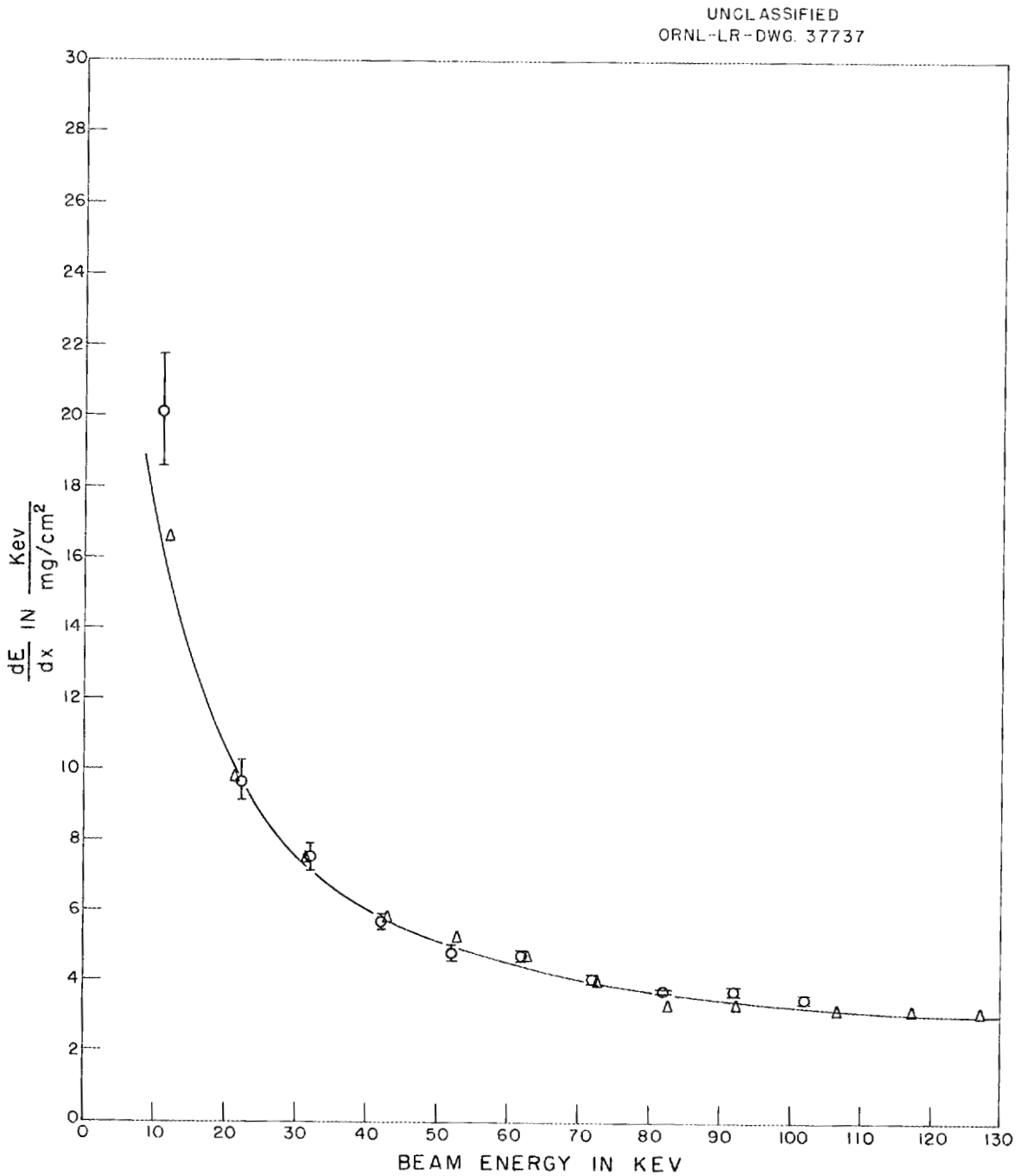

Figure 16. Stopping Power of Aluminum (50.3 μg/cm² Foil) and (107.8 μg/cm² Foil).

VIII. DISCUSSION

In Figure (16) it can be seen that there is very good agreement between the Bethe stopping power theory and the experimental results of this work for the two aluminum foils used. There is no other experimental work with which comparison may be made. That is, the thinnest foil in which electron slowing down has been observed being 1.65 mg/cm^2 or some 15 times thicker than the thickest foil used here. Furthermore, the lowest energy emphasized in this study by Shpinel[26] was 148 KeV, and the principal interest was the straggling distribution. Foils in the mg/cm^2 range have been used in all quantitative studies to date in order to achieve an energy loss large enough to measure by taking the difference (usually comparable to spectrometer resolution) between the incoming and outcoming beam energies. Such thick foil experiments always involve enough multiple scattering to make path length correction to the foil thickness difficult. Furthermore, the angle of acceptance of the typical spectrometer for the emerging electrons is invariably very small. Thus, the energy distributions of only a small fraction of the emerging electrons are studied. In the work reported here the average energy loss itself was measured directly by calorimetric means. Foils used were thin enough to permit a calculation of the path length for the energies used. For example, the increase in path length as calculated by using Equations (36) and (50) were 7.8% and 1.4% at 10 and 20 KeV incident electron energies, respectively for the 50.3 $\mu g/cm^2$ Al foil. The path

[26] V. C. Shpinel, Zhur. Eksper. i. Theor. Fiz. 22, 421 (1952).

length corrections for the 107.8 $\mu g/cm^2$ Al foil were 20.6%, 4.1%, and 1.5% at 10, 20, and 30 KeV incident electron energies, respectively. The amount of heat involved here is readily measured by simple calorimetric techniques. The only limitation on the primary energy which may be investigated is imposed by the thickness of foils which may be made.

IX. CONCLUSIONS

The stopping power of aluminum for electrons having energies of 10 to 125 KeV was studied by measuring the average energy loss directly by calorimetric means. Two different aluminum foils were studied of thicknesses 50.3 and 107.8 micrograms per square centimeter. At these thicknesses the scattering was not excessive for the incident electron energies used. The maximum path length correction was 20.6%. This was for the thickest foil and lowest incident electron energy. The foils were evaporated foils evaporated rapidly so that their thicknesses were uniform.

The maximum measured energy loss was 2.5% of the incident energy and was found for the thicker foil and lowest energy. The minimum measured energy loss was 0.28% of the incident energy. This was for the thinner foil and maximum incident energy.

The experimental results gave excellent agreement with Bethe's stopping power theory for the aluminum foils used after path length corrections were made. Since the stopping power of aluminum oxide would not be much different from that of aluminum, according to theory, then any aluminum oxide coating on the foils would not be expected to affect the results significantly. On the basis of these experimental results, it appears likely that Bethe's stopping power theory is accurate for the energy range studied and for light materials. This is to be expected in that the beam energy was always more than five times the

ionization potential of the deepest electron shell (K shell ionization potential is 1500 volts in Al). It would be interesting to study electron stopping power for energies and atomic numbers where this is not so.

In addition, it would be well to extend the measurements to lower incident electron energies for low Z materials. Since the foils used were near the minimum thickness of self-supporting foils, it will be necessary to use a thin plastic backing for supporting the foil. By using different ratios of foil thickness to the thickness of the plastic backing, the measured stopping power may be extrapolated to give both the stopping power of the metallic foil material and the stopping power of the plastic backing.

APPENDIX

A. Sample Calculation

The sample calculation which follows is for the 50.3 $\mu g/cm^2$ aluminum foil. The procedure to be followed will be to describe in detail the evaluation of $\mathring{T}$ for one of the calibration points at full absorption of the beam, and then the evaluation of the calibration constant which appears in the relationship

$$P_B = \frac{1}{K_1} \mathring{T} \tag{94}$$

Then the $\overline{\Delta E}$ for an incident energy of 11.9 KeV will be determined. The method for obtaining the average foil thickness $\overline{\Delta x}$ with the associated calculations will be given. Then the average increase in path length $\overline{\Delta \ell}$ for 11.9 KeV incident electrons will be calculated. The measured stopping power $\overline{\Delta E}/\overline{\ell}$, where $\overline{\ell}$ is the sum of $\overline{\Delta x}$ and $\overline{\Delta \ell}$, will be calculated for this incident energy of 11.9 KeV.

1. Calibration

Given below in Table II is a tabulation of the data for one of the calibration points at full absorption of the beam.

TABLE II. Data for One Calibration Point

Temp. T cm	T - 20.4	Time t, min	Measured 2nd Anode Potential, volts	Beam Current, μa
20.4	0	0	1500 (0-1500 range)	0.21
21.4	1.0	0.1		
22.3	1.9	0.2		
23.3	2.9	0.3		
24.2	3.8	0.4		
T_o = 25.0	4.6	0.5		
25.9	5.5	0.6		
26.7	6.3	0.7		
27.5	7.1	0.8		
28.4	8.0	0.9		
29.2	8.8	1.0		
TOTALS	49.9	5.5		

$$T = at + b \quad ,$$

A straight line was fitted to these points and the slope "a" is just $\dot{T}$, the quantity to be determined. According to the theory of least squares

$$a = \dot{T} = \frac{n \sum_{i=1}^{n} T_i t_i - \sum_{i=1}^{n} n_i \sum_{i=1}^{n} T_i}{n \sum_{i=1}^{n} t_i^2 - \left(\sum_{i=1}^{n} t_i \right)^2} \tag{95}$$

where n is the number of observations. From the data of Table II above then with n = 11

$$\sum_{i=1}^{n} T_i t_i = 34.56 \quad ,$$

$$\sum_{i=1}^{n} t_i = 5.5 \quad ,$$

$$\sum_{i=1}^{n} t_i^2 = 3.85 \quad ,$$

$$\sum_{i=1}^{n} T_i = 49.9 \quad .$$

Putting these values into Equation (95), then

$$\dot{T} = 8.740 \ \frac{\text{cm}}{\text{min}} \quad . \tag{96}$$

At full absorption, the electron energy is determined by the second anode potential which was measured on the panel meter to be 1500 volts. Using Equation (86) to get the correction to the panel meter reading for the 0-1500 volt range,

$$\begin{aligned} \Delta V &= 0.038\ (1500) + 7 \\ &= 57 + 7 = 64 \text{ volts} \end{aligned} \tag{97}$$

Hence, the beam energy E_B was

$$E_B = (1500 + 64) = 1564 \text{ ev.} \tag{98}$$

The beam power P_B absorbed by the foil at this full absorption was

$$P_B = E_B i_B = 1564 \text{ ev } (0.21\ \mu a)$$
$$= 328.3\ \mu w\ . \tag{99}$$

Tabulated below in Table III are the various beam powers P_B at full absorption along with their corresponding $\dot{T}$.

TABLE III. Calibration Data

$P_B = \mu w$	$\dot{T}$ cm/min
0	0
47.99	0.916
93.02	2.440
140.7	3.750
187.6	4.870
237.6	6.090
328.3	8.740

A plot of P_B versus $\dot{T}$ is made with the straight line fit forced to go through the origin. The points fall well on a straight line as can be seen by referring to Figure (14). The best straight line was fitted to

these points by means of least squares. Consider the slope of this line to be the constant $(K_1)^{-1}$, which is called the calibration constant. The units of $(K_1)^{-1}$ will be microwatts per centimeter per minute so that

$$P_B = K_1^{-1} \dot{T} \tag{100}$$

Now according to the method of least squares, if the curve goes through the origin then the slope $(K_1)^{-1}$ will be given by

$$K_1^{-1} = \frac{\sum_{i=1}^{n} (P_B \dot{T})_i}{\sum_{i=1}^{n} (\dot{T}^2)_i} \tag{101}$$

where n is the number of observations. From the data of Table III,

$$\sum_{i=1}^{n} (P_B \dot{T})_i = 6028.49 \quad ,$$

$$\sum_{i=1}^{n} (\dot{T}^2)_i = 158.05 \quad ,$$

so that $(K_1)^{-1} = 38 \frac{\mu w}{cm/min}$.

2. Determination of $\overline{\Delta E}$

When the beam energy is increased above that for full absorption in the foil, the beam power absorbed in the foil (P_B) will still be given by

$$P_B = (K_1)^{-1} \dot{T} \tag{102}$$

since the temperature monitor is sensitive only to the power absorbed in the foil. In this case, however, the absorbed beam power will be the product of the average energy loss in the foil ($\overline{\Delta E}$) and the beam current (i_B). This incident energy of 11.9 KeV is numerically equal to the sum of potentials of the accelerator and the second anode of the electron gun. When the beam current was 0.150 microamperes at this incident energy of 11.9 KeV, the observed $\dot{T}$, determined by least squares as before, was 3.62 cm/min. Therefore, $\overline{\Delta E}$ is given by

$$\overline{\Delta E} = \frac{P_B}{i_B} = \frac{(K_1)^{-1} \dot{T}}{i_B} = \frac{38(3.62)\ \mu w}{0.150\ \mu a} \tag{103}$$

$$= 913 \text{ ev.}$$

3. Determination of $\bar{\ell}$

The average path length $\bar{\ell}$ is the sum of the average foil thickness $\overline{\Delta x}$ and the average increase in path length $\overline{\Delta \ell}$ produced by scattering. To determine $\overline{\Delta x}$, the foil was punched out with a punch having a diameter of 0.442 inch or 1.12 cm. Thus, the area (A) of the punched foil was

$$A = \pi \frac{d^2}{4} = \frac{3.14}{4} (1.12)^2 = 0.99 \text{ cm}^2 \tag{104}$$

The foil and standard 1, 2, and 3 mg weights were weighed in the modified electrobalance. Weight measurements were actually a measure of the potential drop V across a wire wound resistor in series with the torque motor. In Table IV, these measurements of V are tabulated along with the corresponding weight. The V which is tabulated is the average V for ten successive readings.

TABLE IV. Weight Measurements

Weight W, mg	V_{ave} (mv)
1.000*	118.025
2.000*	231.99
3.000*	346.31
foil**	9.464

The weights designated with the single asterix were N.B.S. Class M weights. Using these weights as calibration points, the constants in the relationship

$$W = aV + b \tag{105}$$

were determined by least squares, where W is the weight in milligrams and V is in millivolts. The data of Table IV gives

$$a = 0.00876 \ \frac{mg}{mv} \tag{106}$$

and

$$b = 0.0333 \text{ mg.} \tag{107}$$

To get the weight of the foil, then

$$\begin{aligned} W &= aV + b \\ &= \left[0.00876\ (9.464) - 0.0333 \right] mg \\ &= \left[0.0828 - 0.0333 \right] mg \\ &= 0.0496 \ mg \\ W(\text{foil}) &= 49.6 \ \mu g \end{aligned} \tag{108}$$

The average foil thickness $\overline{\Delta x}$ in micrograms per square centimeter is given by

$$\overline{\Delta x} = \frac{W(\text{foil})}{A(\text{foil})} = \frac{49.6 \text{ mg}}{0.987 \text{ cm}^2} = 50.3 \ \frac{\mu g}{\text{cm}^2} \tag{109}$$

To calculate the average increase in path length produced by scattering, the simpler scatter theory was used, so that

$$\overline{\Delta \ell} = 1/2 \int_0^t \overline{\theta^2} \, dt \quad , \tag{110}$$

with

$$\overline{\theta^2} = t \, \frac{4\pi N Z(Z+1) \, e^4 \, (1-\beta^2)}{m_o^2 \, v^4} \ln \left[4\pi \, Z^{1/3} \, (Z+1) N t \, \frac{h^2}{m_o v} \right] , \tag{111}$$

and $N = \frac{N_A \rho}{A}$, N_A being Avogadro's number.

Consider for example an incident electron energy of 10 KeV so that

$$v^2 = 0.34 \times 10^{20} \ \frac{\text{cm}^2}{\text{sec}^2} \ ,$$

$$(1-\beta^2) = 0.962 \quad .$$

For simplicity, let

$$\alpha = \frac{4\pi NZ\ (Z+1)\ e^4\ (1-\beta^2)}{m_o^2\ v^4} \quad , \tag{112}$$

$$\text{and} \quad \delta = 4\pi Z^{1/3}\ (Z+1)\ N\ \left(\frac{h}{m_o v}\right)^2 \quad . \tag{113}$$

Thus

$$\overline{\Delta \ell} = 1/2 \int_o^t \alpha t \ln(\delta t) dt = \frac{\alpha}{2} \int_o^t \left[t \ln\delta + t \ln t \right] dt$$

$$= \frac{\alpha}{2} \left[\frac{t^2}{2} \ln \delta + \frac{t^2}{2} \ln t - \frac{t^2}{4} \right]$$

$$= \frac{\alpha t^2}{4} \left[\ln \delta + \ln t - 1/2 \right]$$

$$= \frac{\alpha t^2}{4} \left[\ln \delta\ t - 1/2 \right] \tag{114}$$

Now, for aluminum

$$N = \frac{N_A \rho}{A} = \frac{6.02 \times 10^{23} \times 2.70}{27} = 6.02 \times 10^{22} \ \frac{\text{atoms}}{\text{cc}} \quad ,$$

$$Z = 13,$$

$$\text{and } e = 4.8 \times 10^{-10} \text{ esu},$$

$$m_o = 9.11 \times 10^{-28} \text{ g.}$$

Using these values in Equations (112) and (113), then

$$\alpha = 7.25 \times 10^{3} \text{ cm}^{-1} \quad , \tag{115}$$

$$\delta = 9.5 \times 10^{5} \text{ cm}^{-1} \quad , \tag{116}$$

when the incident energy is 10 KeV. Since we have been considering the 50.3 $\mu g/cm^2$ aluminum foil, then

$$t = \frac{50.3 \ \mu g/cm^2}{2.70 \ g/cm^3} = 1.87 \times 10^{-5} \text{ cm.} \tag{117}$$

Thus $\overline{\Delta \ell}$ given by Equation (114) becomes

$$\begin{aligned} \overline{\Delta \ell} &= 0.154 \times 10^{-5} \text{ cm} \\ &= 4.2 \ \mu g/cm^2 \end{aligned} \tag{118}$$

and hence,

$$\begin{aligned} \overline{\ell} &= \overline{\Delta x} + \overline{\Delta \ell} = (50.3 + 4.2) \ \mu g/cm^2 \\ &= 54.5 \ \mu g/cm^2 \end{aligned} \tag{119}$$

Therefore

$$\frac{\overline{\Delta E}}{\overline{\ell}} = \frac{913 \text{ ev}}{54.5 \ \mu g/cm^2} = 16.7 \ \frac{\text{ev}}{\mu g/cm^2} = 16.7 \ \frac{\text{KeV}}{mg/cm^2} \tag{120}$$

B. Data

Tabulated below are the complete data for the 50.3 and 107.8 $\mu g/cm^2$ aluminum foils in Tables V, VI, and VII. Table V is for the 50.3 $\mu g/cm^2$ aluminum foil. The data of Table VI is for the 107.8 $\mu g/cm^2$ aluminum foil for incident energies of 11.25 to 62 KeV. For this data the calibration constant $(K_1)^{-1}$ was larger than that of Table V because the resistance in series with the temperature monitoring thermocouple was 10Ω rather than 1Ω shown in Figure (8). This decreased the sensitivity of the temperature monitoring galvanometer so that the $\dot{T}$ was lower for a given beam power absorbed. The data of Table VII was for the 107.8 $\mu g/cm^2$ aluminum foil for incident energies of 22 to 102 KeV. In this case the calibration was lower than that of Table V because the temperature monitoring galvanometer G4 shown in Figure (8) was connected directly across the thermocouple. The circuit for zeroing the galvanometer was disconnected. This increased the sensitivity of the galvanometer since there was less resistance in series with it. Thus the $\dot{T}$ was larger for a given beam power absorbed and this resulted in a smaller calibration constant.

TABLE V. Stopping Power Data for the 50.3 $\mu g/cm^2$ Al Foil

$E(Beam)^3$ KeV	$\dot{T}$ cm/min	$P_B = 38\ \dot{T}$ μw	i_B μa	$\overline{\Delta E} = \frac{P_B}{i_B}$ ev	$\langle \frac{dE}{dx} \rangle$ $\frac{KeV}{mg/cm^2}$ Exp	Theory
11.9	3.62	137	0.150	913	16.7	15.0
22.1	2.00	76.0	0.152	500	9.77	9.75
32.3	1.50	57.0	0.152	375	7.45	7.10
42.6	1.15	43.7	0.151	289	5.74	5.75
52.8	0.63	23.8	0.090	264	5.25	4.98
	1.26	47.9	0.182	263	5.23	
	1.83	69.6	0.270	258	5.13	
					Ave. 5.20	
62.9	1.65	62.7	0.270	232	4.62	4.40
72.9	1.40	53.2	0.270	197	3.91	3.90
82.8	1.22	46.3	0.270	172	3.42	3.60
	1.09	41.4	0.269	154	3.06	
					Ave. 3.24	
92.6	1.05	39.9	0.269	148	2.94	3.35
	1.14	43.3	0.270	160	3.18	
	1.28	48.6	0.270	178	3.54	
					Ave. 3.22	
106.8	2.42	92.0	0.605	152	3.02	3.17
	1.50	57.0	0.350	163	3.24	
					Ave. 3.13	
116.8	1.23	46.7	0.305	153	3.04	3.11
	2.08	79.0	0.495	159	3.16	
					Ave. 3.10	
127.2	0.374	14.2	0.090	158	3.14	3.06
	0.791	30.1	0.180	167	3.32	
	1.05	39.9	0.270	148	2.94	
	2.79	106.	0.705	151	3.00	
	2.69	102.	0.700	145	2.88	
					Ave. 3.05	

TABLE VI. Stopping Power Data for the 107.8 μg cm^2 Al Foil

E(Beam) KeV	$\dot{T}$ cm/min	$P_B = 47.1\ \dot{T}$ μw	i_B μa	$\overline{\Delta E} = \frac{P_B}{i_B}$ ev	$\langle \frac{dE}{dx} \rangle$, $\frac{KeV}{mg/cm^2}$ Exp.
11.25	1.33	65.1	0.0255	2552	19.20
	1.20	58.9	0.0206	2858	21.50
					Ave. 20.3 ± 1.32*
22	1.20	58.5	0.0572	1023	9.06
	1.93	93.0	0.0824	1129	10.00
					Ave. 9.53
32	2.40	115.3	.148	777	7.06
	1.15	56.4	.064	886	8.06
	4.30	204.8	.238	860	7.82
					Ave. 7.65
42	1.99	96.0	.156	616	5.72
	3.80	181.2	.311	584	5.41
					Ave. 5.56
52	3.60	171.5	.322	533	4.94
	1.80	87.0	.159	546	5.07
					Ave. 5.00
62	2.09	100.6	.192	523	4.85
	3.56	169.7	.324	525	4.87
					Ave. 4.86

* Probable Error.

TABLE VII. Stopping Power Data for the 107.8 $\mu g/cm^2$ Al Foil

E(Beam) KeV	$\dot{T}$ cm/min	$P_B = 28.1\ \dot{T}$ μw	i_B μa	$\overline{\Delta E} = \frac{P_B}{i_B}$ ev	$\langle \frac{dE}{dx} \rangle$, $\frac{KeV}{mg/cm^2}$ Exp.
22	7.40	209	0.191	1090	9.67 Ave. 9.56 ± 0.33*
32	10.54	2.97	0.396	750	6.83 Ave. 7.40 ± 0.41
42	3.88	110	0.170	648	6.01 Ave. 5.71 ± 0.20
52	5.34	151	0.312	483	4.48 Ave. 4.83 ± 0.21
62	6.10	172	0.342	504	4.68 Ave. 4.80 ± 0.09
72	5.20 5.38 3.29	147 152 93	0.342 0.350 0.203	430 435 461	3.99 4.03 4.28 Ave. 4.10 ± 0.10
82	2.88 5.35 5.34	82 151 151	0.204 0.371 0.372	403 407 405	3.74 3.78 3.76 Ave. 3.76 ± 0.02
92	5.50 5.17 2.75	155 146 78	0.364 0.368 0.204	427 397 384	3.96 3.68 3.56 Ave. 3.74 ± 0.14
102	4.82 4.98 2.50	136 141 71	0.367 0.360 0.189	371 391 377	3.45 3.63 3.50 Ave. 3.53 ± 0.10

* The averages include the data of Table VI. The error is the probable error.

C. Error Analysis

The current measuring apparatus was calibrated before and after each day's work. The measurements of the beam current were accurate to about 1.5%. The panel meter used for measuring the accelerator potential was a 2% meter which was calibrated as described previously. The second anode potential of the electron gun was also calibrated as described earlier. Since the second anode potential determined the beam energy at full absorption of the beam during the calibration, the accuracy of the calibration depended on a knowledge of the second anode potential. Both potentials were assumed to be known to within 2%.

The foil thickness depended on the weight of and area of the punched out foil to determine the foil thickness in micrograms per square centimeter. The diameter of the punch used for punching out the foil was measured to one part in 400. It was found that by weighing the foil above, and then weighing it with one or more National Bureau of Standards, Class M weights, that differences of no more than 1 microgram were found. Assuming the standard weights to be exact, and using the average of the weight measurements, the foil weight was accurate to within 1%. Thus the foil thickness in micrograms per square centimeter was accurate to within 1%.

In measuring the rate of temperature drift for a given beam power absorbed by the foil, the measurements depended on how accurately the galvanometer scale can be read as the galvanometer drifted. The times at which the measurements were made were as accurate as the 60 cycle frequency of the AC voltage inasmuch as a sychronous motor (10 revolutions per minute) was used to trigger a buzzer every 0.1 minute. The buzzer sound was the signal for making a temperature measurement and thus the limitation on timing accuracy was human reaction time. Since the galvanometer used in these measurements had a gold fiber suspension and was exposed to room temperature variations extraneous thermocouple effects were introduced. However, these latter effects were small since the galvanometer usually drifted back to its original zero position after each run. When the galvanometer did not drift back to near its zero position, then the data was discarded for that run.

The probable error[27] is 0.67 times the standard deviation, where

$$\sigma^2 = \frac{\sum_{i=1}^{n} (\bar{x} - x_i)^2}{n - 1} , \qquad (121)$$

Here n is the number of observations, and $\bar{x}$ the average value of the observations. Consider $\bar{x}$ to be the average measured stopping power

[27] Yardley Beers, INTRODUCTION TO THE THEORY OF ERROR (Addison-Wesley, Cambridge, Mass., 1953).

of the 107.8 $\mu g/cm^2$ aluminum foil for 32 KeV electrons and the x_i to be the individual observation. If one uses the data of Tables VI and VII, then

$$\bar{x} = 7.40 \ \frac{\text{KeV}}{\text{mg/cm}^2} \tag{122}$$

and

$$(\bar{x}-x_1)^2 = (7.40 - 7.06)^2 = 0.116 \quad ,$$

$$(\bar{x}-x_2)^2 = (7.40 - 8.06)^2 = 0.435 \quad ,$$

$$(\bar{x}-x_3)^2 = (7.40 - 7.82)^2 = 0.176 \quad ,$$

$$(\bar{x}-x_4)^2 = (7.40 - 6.83) = 0.396 \quad ,$$

Thus

$$\sigma^2 = \frac{1.123}{3} = 0.374 \quad , \tag{123}$$

and the probable error (P.E.) is

$$\text{P.E.} = 0.67 \ (0.374)^{1/2} = 0.41 \quad . \tag{124}$$

Thus the relative probable error determined in this manner was

$$\frac{P.E.}{\bar{x}} = \frac{0.41}{7.40} = 5.5\% \quad . \tag{125}$$

The errors associated with the various experimental quantities have been evaluated previously. Errors in the measurements of i_B, the beam energy during a run, the same during calibration, and foil thickness were respectively 1.5%, 2%, 2%, and 1%. Since these errors are independent, then the over-all error of these factors is the square root of the sum of the squares of each individual error, i.e.,

$$\text{over-all error} = \left[(0.015)^2 + (0.02)^2 + (0.02)^2 + (0.01)^2 \right]^{1/2}$$

$$= 0.034 = 3.4\% . \tag{126}$$

D. List of Symbols Used

Listed below in alphabetical order are the symbols used in this work. The c.g.s. system of units was used unless otherwise specified.

a = effective atomic shielding radius = $a_o Z^{-1/3}$.

a_o = Bohr radius = 5.29×10^{-9} cm.

$\alpha = \frac{Ze^2}{hv} = \frac{Z}{137\,\beta}$.

β = v/c where v is the electron velocity and c is the velocity of light.

b = impact parameter, the closest distance of approach of two colliding particles if there were no force of interaction.

b_{max} = maximum impact parameter at which an energy transfer can occur in the electron-electron collision.

b_{min} = minimum impact parameter in an electron-electron collision.

c = velocity of light $\cong 3 \times 10^{10}$ cm/sec.

$(K_1)^{-1}$ = calibration constant in $\frac{\mu \text{ watts}}{\text{cm/min}}$, which appears in the relationship $P_B = (K_1)^{-1} \dot{T}$.

γ = Lorentz factor = $(1 - \beta^2)^{1/2}$.

E_{bias} = bias potential applied to bias discs on either side of the foil for repelling secondary electrons back into the foil.

$\overline{\Delta E}$ = average energy lost by the incident electrons in the foil, in units of electron-volts.

e = electronic charge = 4.8×10^{-10} esu.

ϵ = base of the natural logarithms = 2.71828

$f(\theta, dx)d\theta$ = probability for a single nuclear scattering between θ and $\theta + d\theta$.

G4 denotes the galvanometer used in monitoring the foil temperature.

$\hbar$ = Planck's constant/2π = 1.04×10^{-27} erg-sec.

i_B = current of the electron beam striking the foil in microamperes.

i_4 = Peltier cooling current, i.e., the current sent through the cooling thermopile for precooling the foil below its environmental temperature.

I = mean ionization potential of an absorber; 150 ev for Al.

K = thermal conductivity

K_1, K_2 = proportionality constants which appear in the relationship

$$T = K_1 P_B - K_2 (T - T_o).$$

K_1 is in units of $\frac{cm/min}{\mu w}$.

K_2 is in units of min^{-1}.

$\bar{\ell}$ = average path length of the electrons going through the foil.

$d\ell$ = increase in path length produced by a single scattering.

$\overline{\Delta\ell}$ = average increase in path length over the entire thickness of the absorber.

m_o = electronic rest mass = 9.11×10^{-28} g.

N_A = Avogadro's number = 6.02×10^{23} atoms/mole.

N = number of atoms per cubic centimeter = $\frac{N_A \rho}{A} = \frac{6.02 \times 10^{23} \times 2.69}{26.97} =$

6.02×10^{22} atoms/cc for Al.

P_B = $i_B \overline{\Delta E}$ = power lost by the incident electron beam in the foil in units of micro-watts.

ds = increment of path taken by the scattered electron between collisions.

$d\sigma(\theta)$ = Rutherford differential cross section per atom for scattering into a solid angle $d\Omega$.

θ_{max} = maximum scattering angle in a single collision of the incident electron with a nucleus.

θ_{min} = minimum scattering angle in a nuclear collision.

dt = increment of foil thickness.

t = either the foil thickness or time

t_o = time at which $T = T_o$.

T = temperature (usually the foil temperature) measured in centimeters of deflection of the temperature monitoring galvanometer.

T_o = temperature of the environment and the thermopile reference junctions.

T_∞ = foil temperature at time $t \to \infty$.

T_+ = foil temperature at time $t = t_o + \Delta t$.

T_- = foil temperature at time $t = t_o - \Delta t$.

T_i = initial temperature of the foil prior to heating it by the electron beam.

Bibliography

Beers, Yardley, INTRODUCTION TO THE THEORY OF ERROR, (Addison-Wesley, Cambridge, Mass., 1953).

Bethe, H., Ann. Phys. 5, 325 (1930).

Bethe, H. A., Handbuch der Physik, Bd. 24, (1933).

Birkhoff, R. D., Handbuch der Physik, 34, 53 (1958).

Blackstock, A. W., R. D. Birkhoff, and M. Slater, Rev. Sci. Inst. 26, 274 (1955).

Bloch, F., Z. Phys. 81, 363 (1933).

Blunck, O., and S. Leisegang, Z. Phys. 128, 500 (1950).

Bothe, W., Handbuch der Physik, 22, 2 (1933).

Brandt, W., Health Physics 1, 11 (1958).

Brandt, W., Phys. Rev. 104, 691 (1956).

Frazen, W., and L. Schellenberg, Rev. Sci. Inst. 27, 171 (1956).

Holland, L., VACUUM DEPOSITION OF THIN FILMS (Chapman and Hall, Ltd. London, 1956).

Jensen, H., Z. Phys. 106, 620 (1937).

Landau, L., J. Phys. USSR, 8, 201 (1944).

Leithanser, E., Ann. Phys. 15, 283 (1904).

Molière, G., Z. Naturforsch 3a, 78 (1948).

Rothwell, P., Proc. Phys. Soc. Lond. 64, 911 (1951).

Shpinel, V. C., Zhur. Eksper. i. Theor. Fiz. 22, 421 (1952).

Warshaw, S. D., Rev. Sci. Inst. 20, 623 (1940).

West, D., Proc. Phys. Soc. Lond. 66, 306 (1953).

Whiddington, R., Proc. Roy. Soc. Lond. Ser. A-86, 360 (1912).

Williams, E. J., Proc. Roy. Soc. Lond. Ser. A-169, 531 (1939).

Williams, E. J., Phys. Rev. 58, 292 (1940).

INTERNAL DISTRIBUTION

1. C. E. Center
2. Biology Library
3. Health Physics Library
4-5. Central Research Library
6. Reactor Experimental Engineering Library
7-26. Laboratory Records Department
27. Laboratory Records, ORNL R.C.
28. L. B. Emlet (K-25)
29. J. P. Murray (Y-12)
30. A. M. Weinberg
31. J. A. Swartout
32. E. D. Shipley
33. M. L. Nelson
34. K. Z. Morgan
35. S. C. Lind
36. A. S. Householder
37. C. S. Harrill
38. C. E. Winters
39. A. H. Snell
40. E. H. Taylor
41. W. H. Jordan
42. T. A. Lincoln
43. A. Hollaender
44. F. L. Culler
45. H. E. Seagren
46. D. Phillips
47. M. T. Kelley
48. E. E. Anderson
49. R. S. Livingston
50. C. P. Keim
51. K. E. Cowser
52. C. D. Susano
53. L. B. Farabee
54. F. J. Davis
55. R. J. Morton
56. C. E. Haynes
57. E. G. Struxness
58. W. E. Cohn
59-109. H. H. Hubbell, Jr.
110. D. E. Arthur
111. J. Neufeld
112. M. J. Skinner
113. J. C. Hart
114. T. H. J. Burnett
115. W. J. Lacy
116. G. S. Hurst
117. T. E. Bortner
118. J. A. Lane
119. P. M. Reyling
120. C. E. Clifford
121. J. L. Gabbard
122. R. A. Charpie
123. D. M. Davis
124. P. E. Brown
125. E. D. Gupton
126. J. C. Ledbetter
127. R. L. Clark
128. G. C. Cain
129. L. C. Johnson
130. W. W. Ogg
131. O. D. Teague
132. E. L. Sharp
133. E. J. Kuna
134. H. H. Abee
135. C. R. Guinn
136. A. D. Warden
137. C. C. Sartain
138. J. R. Muir
139. J. A. Auxier
140. M. F. Fair
141. S. I. Auerbach
142. G. W. Royster, Jr.
143. R. R. Dickison
144. F. W. Sanders
145. F. C. Maienschein
146. W. J. Boegly, Jr.
147. F. L. Parker
148. W. E. Lotz
149. B. Fish
150. M. B. Edwards
151. F. M. Empson
152. G. G. Robeck
153-202. R. D. Birkhoff
203. R. H. Ritchie
204. J. A. Harter
205. R. M. Johnson
206. J. S. Cheka
207. P. N. Hensley
208. R. W. Peelle
209. D. R. Nelson
210. E. B. Wagner
211. C. A. Preskitt
212. J. C. Frye (consultant)

213. R. L. Platzman (consultant)
214. A. Wolman (consultant)
215. R. Zirkle (consultant)
216. L. S. Taylor (consultant)
217. ORNL - Y-12 Technical Library, Document Reference Section

EXTERNAL DISTRIBUTION

218. Knolls Atomic Power Laboratory, Schenectady (Robert J. Feinberg)
219. Capt. J. C. Villforth, 58 Diana Lane, West, Fairbarn, Ohio
220. W. O. Olson, 328 Liberty Street, Mankato, Minnesota
221. A. P. Hull, Industrial Reactor Laboratories, Inc., Plainsboro, N.J.
222. Lester Scaggs, Argonne Cancer Research Hospital, Chicago 37, Illinois
223-227. W. G. Stone, Redstone Arsenal, Huntsville, Alabama
228-237. F. Kalil, 314 Grovethorn Road, Baltimore 20, Maryland
238. J. S. Laughlin, Dept. of Physics, Memorial Center, Sloan-Kettering, New York 21, New York
239. S. Berk, 1334, Frankford Arsenal, Philadelphia 37, Pennsylvania
240. W. B. Mann, National Bureau of Standards, Chief, Radioactivity Section, Washington 25, D. C.
241. W. C. Roesch, 2413 Tinkle Street, Richland, Washington
242. G. D. Adams, Jr., Radiological Laboratory, University of California Medical Center, San Francisco 22, California
243. Division of Research and Development, AEC, ORO
244-780. Given distribution as shown in TID-4500 (14th ed.) under Physics and Mathematics category